Title

Differential encoding of mammalian proprioception by voltage-gated sodium channels

Journal

Science Advances, 11(2)

ISSN

2375-2548

Authors

Espino, Cyrrus M

Nagaraja, Chetan

Ortiz, Serena

et al.

Publication Date

2025-01-10

DOI

10.1126/sciadv.ads6660

Peer reviewed

NEUROSCIENCE

Differential encoding of mammalian proprioception by voltage-gated sodium channels

Cyrrus M. Espino[1], Chetan Nagaraja[1], Serena Ortiz[2], Jacquelyn R. Dayton[1], Akash R. Murali[1,3], Yanki Ma[1,3], Emari L. Mann[1,4], Snigdha Garlapalli[1,5], Ross P. Wohlgemuth[6], Sarah E. Brashear[6], Lucas R. Smith[6], Katherine A. Wilkinson[2], Theanne N. Griffith[1]*

Animals requiring purposeful movement for survival are endowed with mechanoreceptors, called proprioceptors, that provide essential sensory feedback from muscles and joints to spinal cord circuits, which modulates motor output. Despite the essential nature of proprioceptive signaling in daily life, the mechanisms governing proprioceptor activity are poorly understood. Here, we identified nonredundant roles for two voltage-gated sodium channels (Na_Vs), $Na_V1.1$ and $Na_V1.6$, in mammalian proprioception. Deletion of $Na_V1.6$ in somatosensory neurons ($Na_V1.6^{cKO}$ mice) causes severe motor deficits accompanied by loss of proprioceptive transmission, which contrasts with our previous findings using similar mouse models to target $Na_V1.1$ ($Na_V1.1^{cKO}$). In $Na_V1.6^{cKO}$ animals, we observed impairments in proprioceptor end-organ structure and a marked reduction in skeletal muscle myofiber size that were absent in $Na_V1.1^{cKO}$ mice. We attribute the differential contributions of $Na_V1.1$ and $Na_V1.6$ to distinct cellular localization patterns. Collectively, we provide evidence that Na_Vs uniquely shape neural signaling within a somatosensory modality.

INTRODUCTION

Proprioception, often referred to as our "sixth sense," is a largely unconscious sensation that allows for the detection of one's own body position and movement in space (*1*, *2*). Proprioceptive signaling is initiated by a subclass of peripheral mechanosensory neurons, called proprioceptors, whose cell bodies reside in the dorsal root ganglia (DRG) or mesencephalic trigeminal nucleus (*1*, *3*, *4*). The peripheral axons of proprioceptors innervate skeletal muscle and form mechanosensitive end organs, referred to as muscle spindles and Golgi tendon organs, which are activated by changes in muscle length or force, respectively (*1*). In proprioceptors, the mechanosensitive ion channel Piezo2 transduces changes in muscle movement into electrical signals that give rise to sustained trains of action potentials, which are subsequently transmitted to spinal cord circuits (*4*, *5*). Patients harboring Piezo2 loss-of-function (LOF) mutations have impaired proprioception in the absence of visual input (*6*). Recently, we determined that the voltage-gated sodium channel (Na_V), $Na_V1.1$, is also essential for mammalian proprioception and plays a specific role in maintaining proprioceptor firing during sustained muscle stretch (*7*). Furthermore, we determined $Na_V1.1$ to be haploinsufficient for proprioceptor function and motor behaviors, which is consistent with the clinical manifestations associated with the thousands of human disease-causing mutations associated with its gene, *Scn1a*. Unexpectedly, $Na_V1.1$ was not required for muscle proprioceptor responses to dynamic muscle movement or vibration. This raises the question as to whether Na_Vs play distinct roles in encoding proprioceptive signals.

In addition to $Na_V1.1$, proprioceptors also express $Na_V1.6$ and $Na_V1.7$ (*7*). $Na_V1.7$ is most notable for its role in pain signaling, whereby gain-of-function (GOF) or LOF mutations in *Scn9a*, the gene encoding $Na_V1.7$, cause congenital hypersensitivity or insensitivity to pain, respectively (*8*, *9*). Mice and humans lacking $Na_V1.7$, however, do not have reported motor deficits, indicating a limited role for this channel in proprioception at the behavioral level (*9*, *10*). Conversely, the gene encoding $Na_V1.6$, *Scn8a*, is linked to various pathophysiological conditions associated with motor impairments, such as developmental epileptic encephalopathy and ataxia (*11*). Furthermore, global inactivation of *Scn8a* in mice leads to hindlimb paralysis and death by postnatal day 21 (P21) (*12*). In cerebellar Purkinje neurons, loss of $Na_V1.6$ significantly reduces spontaneous activity and leads to impairments in motor coordination (*13*). While these data highlight critical roles for $Na_V1.6$ in brain-mediated motor control, $Na_V1.6$ function remains understudied in the peripheral nervous system, and how this channel contributes to proprioception is unknown. Understanding the unique contributions of Na_Vs to peripheral proprioception will enhance our mechanistic understanding of the sensorimotor phenotypes associated with various Na_V channelopathies.

In the present study, we set out to determine whether Na_Vs plays distinct or redundant roles in proprioceptive signaling, focusing on the contributions of $Na_V1.1$ and $Na_V1.6$. The use of a *Pvalb-Cre* mouse line to drive Na_V deletion in proprioceptors is not feasible due to parvalbumin expression in the brain and spinal cord (*7*, *14*, *15*). Thus, we used a somatosensory-neuron wide genetic targeting strategy to conditionally deleted $Na_V1.6$ ($Pirt^{Cre/+}$;$Scn8a^{fl/fl}$, $Na_V1.6^{cKO}$) and found that this resulted in severe impairments in motor coordination that were phenotypically distinct from those that we previously observed in mice lacking $Na_V1.1$ in somatosensory neurons [$Pirt^{Cre/+}$;$Scn1a^{fl/fl}$, $Na_V1.1^{cKO}$; (*7*)]. In line with behavioral observations, ex vivo proprioceptor muscle-nerve recordings showed afferent excitability in response to both dynamic and static muscle movements was abolished in the absence of $Na_V1.6$, which contrasts with our prior finding of a selective role for $Na_V1.1$ in proprioceptor encoding of static muscle stretch. Electrophysiological recordings

[1]Department of Physiology and Membrane Biology, University of California, Davis, Davis, CA, USA. [2]Department of Biological Sciences, San José State University, San Jose, CA, USA. [3]Undergraduate Program in Neurobiology, Physiology and Behavior, University of California, Davis, Davis, CA, USA. [4]Postbaccalaureate Research Education Program at UC Davis, University of California, Davis, Davis, CA, USA. [5]Undergraduate Program in Psychology, University of California, Davis, Davis, CA, USA. [6]Department of Physiology, Neurobiology, and Behavior, University of California, Davis, Davis, CA, USA.
*Corresponding author. Email: tgriffith@ucdavis.edu

of the proprioceptor-mediated monosynaptic reflex in the spinal cord further confirmed an essential, albeit developmentally dependent, role for $Na_V1.6$ in proprioceptor synaptic function, whereas $Na_V1.1$ was found to be dispensable. $Na_V1.6^{cKO}$ mice also exhibited abnormal muscle spindle end organ structure, which was not observed in $Na_V1.1^{cKO}$ mice, suggesting that severely but not moderately impaired proprioceptive signaling interferes with proprioceptor end organ development. Unexpectedly, we also observed non–cell-autonomous deficits in skeletal muscle in $Na_V1.6^{cKO}$ mice, but not $Na_V1.1^{cKO}$ mice, that are suggestive of blocked hypertrophy during development. Last, cellular localization experiments found that $Na_V1.1$ and $Na_V1.6$ occupy discrete excitable domains in proprioceptor muscle spindles, which we predict underlies their unique roles in electrical transmission.

Collectively, our findings reveal that $Na_V1.1$ and $Na_V1.6$ are both essential to proprioceptive signaling but have independent and nonredundant functions. The differential contribution of $Na_V1.1$ and $Na_V1.6$ to the activity of individual somatosensory neuron subtypes has not been directly interrogated, and we hypothesize that our findings are broadly applicable to other somatosensory neurons that rely on these channels for neuronal signaling.

RESULTS

Genetic ablation of $Na_V1.6$ in sensory neurons leads to profound motor coordination deficits

To examine the in vivo role of $Na_V1.6$ in sensory-driven motor behaviors, we generated a mouse line in which $Na_V1.6$ is deleted in all peripheral sensory neurons: $Pirt^{Cre/+}Scn8a^{fl/fl}$ (hereafter referred to as $Na_V1.6^{cKO}$), an approach that we previously used to investigate $Na_V1.1$ function in proprioception (*7*). While not selective to proprioceptors, this approach avoids off-target effects on the central nervous system, which include premature death and seizures (*14*). $Na_V1.6^{cKO}$ mice displayed extreme motor deficits that were absent in mice, retaining a single copy ($Na_V1.6^{het}$) or both copies ($Na_V1.6^{fl/fl}$) of *Scn8a* (Fig. 1). Motor deficits included abnormal hindlimb position when suspended by the tail (Fig. 1, A to C, top; and movie S1) or when placed on a flat surface (Fig. 1, A to C, bottom; and movie S2) and an inability to use the tail to guide movements. The motor phenotype produced by $Na_V1.6$ deletion was more severe than the phenotype that we observed following deletion of $Na_V1.1$ in sensory neurons [$Pirt^{Cre/+};Scn1a^{fl/fl}$, $Na_V1.1^{cKO}$; (*7*)]. However, $Na_V1.6^{cKO}$ mice did not display the tremor-like movements that we previously observed in $Na_V1.1^{cKO}$ animals, highlighting a behaviorally distinct phenotype between the two models. We quantified spontaneous locomotion in the open-field and found that $Na_V1.6^{cKO}$ animals traveled significantly less distance (Fig. 1D), on average, walked at slower speeds (Fig. 1E), and reached slower maximal speeds (Fig. 1F), compared to $Na_V1.6^{het}$ and $Na_V1.6^{fl/fl}$ animals. Conversely, maximum acceleration was not different between $Na_V1.1^{fl/fl}$, $Na_V1.1^{het}$, and $Na_V1.1^{cKO}$ animals (fig. S1A). There were no genotype-dependent differences in time spent moving or in the center for the $Na_V1.6$ conditional knockout line (fig. S1, B and C), consistent with our previous finding in the $Na_V1.1$ conditional knockout line (*7*). Furthermore, we did not observe any sex-dependent differences between genotypes (fig. S1 D to F). Using a grip strength meter, we quantified grip force when all four paws were placed on a metal grid and found that $Na_V1.6^{cKO}$ animals had a significantly reduced grip strength compared to other genotypes (Fig. 1G). We next assessed motor coordination using the rotarod; however, the severe motor phenotype of $Na_V1.6^{cKO}$ mice

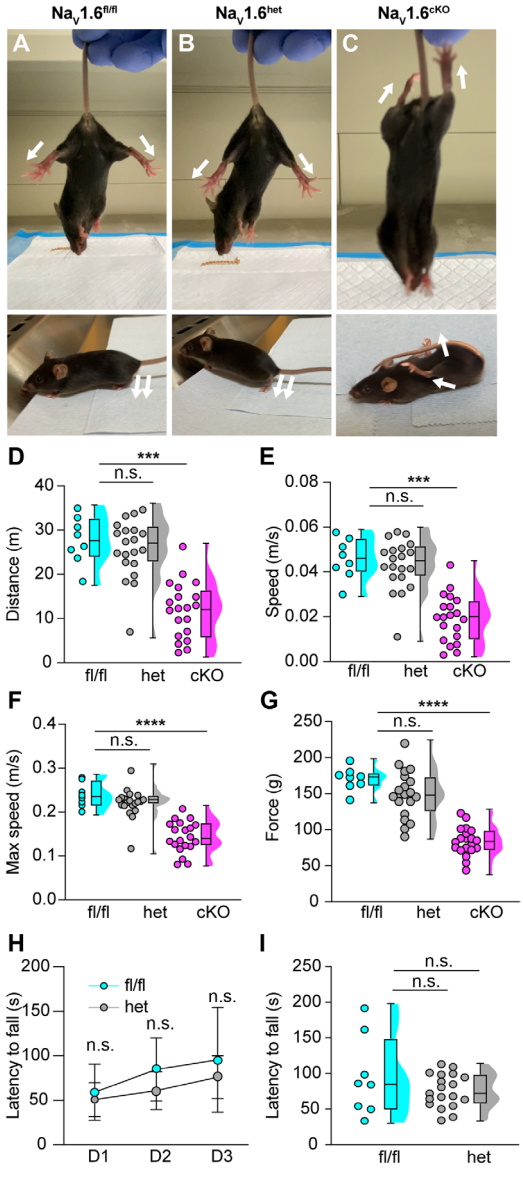

Fig. 1. $Na_V1.6$ is required for somatosensory neuron–driven motor behaviors and function. Representative images showing limb position of adult $Na_V1.6^{fl/fl}$ (**A**), $Na_V1.6^{het}$ (**B**), and $Na_V1.6^{cKO}$ (**C**) mice suspended from the tail (above) and on flat surface (below). White arrows indicate the direction of hindlimbs. Quantification of distance traveled [(**D**), $Na_V1.6^{het}$ ($P > 0.999$) and $Na_V1.6^{cKO}$ ($P = 0.0003$) compared to $Na_V1.6^{fl/fl}$], average speed [(**E**), $Na_V1.6^{het}$ ($P > 0.999$) and $Na_V1.6^{cKO}$ ($P = 0.0003$)], and the maximum speed [(**F**), $Na_V1.6^{het}$ ($P > 0.999$) and $Na_V1.6^{cKO}$ ($P > 0.0001$) compared to $Na_V1.6^{fl/fl}$] for $Na_V1.6^{fl/fl}$ (cyan), $Na_V1.6^{het}$ (gray), and $Na_V1.6^{cKO}$ (magenta) mice as measured in the open-field assay for a 10-min testing period. (**G**) Average grip force in grams measured across six consecutive trials; $Na_V1.6^{het}$ ($P = 0.4947$) and $Na_V1.6^{cKO}$ ($P < 0.0001$) compared to $Na_V1.6^{fl/fl}$. (**H**) Average latency to fall from the rotarod across three consecutive training days. No statistically significant genotype-dependent difference was observed ($P = 0.1342$). (**I**) Average latency to fall on third day of testing [$Na_V1.6^{het}$ ($P = 0.3943$) compared to $Na_V1.6^{fl/fl}$]. Each dot represents one animal, except in (H) were each dot represents the mean across animals. Box and whisker plots represent maximum, minimum, median, and upper and lower quartiles of datasets. A Kruskal-Wallis test with Dunn's multiple comparisons [(D) to (G)], a two-way analysis of variance (ANOVA) with Šidák's multiple comparisons (H), and a Welch's *T* test (I) were used to determine statistical significance. $Na_V1.6^{fl/fl}$, $N = 8$; $Na_V1.6^{het}$, $N = 20$; and $Na_V1.6^{cKO}$, $N = 20$. n.s., not significant.

precluded their testing in this assay. We did not observe genotype-dependent differences in latency to fall between $Na_V1.6^{het}$ and $Na_V1.6^{fl/fl}$ animals across training days (Fig. 1H) or on the final day of testing (Fig. 1I). Collectively, these data show that genetic ablation of $Na_V1.6$ in sensory neurons leads to severe motor deficits that are distinct to those due to $Na_V1.1$ deletion. We previously reported that $Na_V1.1$ was haploinsufficient in sensory neurons for motor behaviors; however, our current results suggest that a single copy of $Na_V1.6$ is sufficient to drive normal behaviors in these motor assays. Nevertheless, we did observe $Na_V1.6$ haploinsufficiency at the afferent level.

$Na_V1.6$ is required for transmission of proprioceptive signals from muscle spindle afferents

Our prior work found that $Na_V1.1$ plays a key role maintaining muscle afferent activity only during static muscle stretch (*7*). Deletion of $Na_V1.1$ had no effect on muscle afferent responses to dynamic muscle movement or vibratory stimuli. To test whether $Na_V1.6$ serves a similarly specific role in proprioceptive transmission, we used an ex vivo muscle nerve preparation to investigate proprioceptor activity from muscle spindle afferents (*16*). First, we tested afferent firing in response to a series of ramp and hold stretches (Fig. 2). Afferents from $Na_V1.6^{fl/fl}$ mice displayed consistent firing throughout the duration of a 4-s ramp and hold stretch protocol and had a high likelihood of resting discharge (Fig. 2A), consistent with wild-type group Ia and II proprioceptor responses. Afferents from $Na_V1.6^{het}$ mice had a similar prevalence of resting discharge compared to those from $Na_V1.6^{fl/fl}$ mice and did not exhibit any significant differences in firing during ramp and hold stretches (Fig. 2B). Notably, afferents from $Na_V1.6^{cKO}$ mice did not have resting discharge and afferent excitability during ramp and hold stretches were nearly abolished (Fig. 2C). In 6 of the 10 mice tested, no stretch-sensitive electrical activity was observed despite the muscle exhibiting healthy twitch contractions. In the four $Na_V1.6^{cKO}$ afferents with stretch-induced firing, it tended to be very sparse and occurred primarily near the beginning of stretch, especially at lower stretch lengths. We quantified afferent properties by examining instantaneous firing frequencies and found a significant reduction in firing at the end of the ramp and hold protocol in $Na_V1.6^{cKO}$ afferents compared to that in $Na_V1.6^{fl/fl}$ afferents across all stretch lengths (Fig. 2D). There were no significant genotype-dependent differences in firing between $Na_V1.6^{het}$ and $Na_V1.6^{fl/fl}$ afferents. We also quantified the regularity of afferent firing by measuring the coefficient of variation of the interspike interval (ISI CV; measured at 1.5 to 3.5 s of the stretch protocol). We only observed firing near the beginning of muscle stretch in two $Na_V1.6^{cKO}$ afferents at 2.5 and 5% of optimal length (Lo), and, in four $Na_V1.6^{cKO}$ afferents at 7.5% of Lo, we observed sparse firing throughout stretch. ISI CV was similar between $Na_V1.6^{fl/fl}$ and $Na_V1.6^{het}$ afferents but was significantly higher in $Na_V1.6^{cKO}$ afferents (Fig. 2E). Together, these findings provide strong evidence that $Na_V1.6$ is required for proprioceptor encoding of static stretch.

Given that $Na_V1.1$ only contributes to proprioceptor afferent firing in response to static muscle stretch, we next asked whether this was also true for $Na_V1.6$. Afferents were tested using a series of sinusoidal vibration protocols at varying frequencies and stimulus amplitudes. In line with the absence of electrical activity during static stretch, $Na_V1.6$ afferents were completely unable to entrain to vibratory stimuli regardless of stimulus amplitude and frequency (Fig. 3). Logistic regression analyses of entrainment probability found that, compared to $Na_V1.6^{fl/fl}$ afferents, afferents from $Na_V1.6^{het}$ animals were significantly less likely to entrain sinusoidal waves ($P < 0.001$; Fig. 3, A and B). This analysis could not be used to assess entrainment probability in $Na_V1.6^{cKO}$ afferents because these afferents never entrained to vibration. Consistent with logistic regression analyses, quantification of the instantaneous firing frequency at 25-μm amplitude vibrations found significant impairments in the ability of $Na_V1.6^{het}$ afferents to respond to vibration, consistent with the notion that $Na_V1.6$ is partially haploinsufficient at the proprioceptor afferent level (Fig. 3D). Thus, unlike $Na_V1.1$ that only serves a role in maintaining proprioceptor responses to static stretch, we find that $Na_V1.6$ plays a direct role in transmitting both dynamic and static muscle movements.

$Na_V1.6$ is essential for proprioceptor synaptic transmission in a developmentally dependent manner

Electrical signals initiated at proprioceptive end organs in skeletal muscle are transmitted to central circuits in the spinal cord. Specifically, proprioceptor Ia afferents directly synapse with alpha motor neurons, comprising the monosynaptic reflex response (*17*, *18*). This spinal circuit provides a tractable model to assess proprioceptor synaptic transmission. Our current results demonstrate that $Na_V1.6$ plays a central role in sensory transmission from muscle spindles; thus, we next asked whether the peripheral deficits that we observed in ex vivo muscle nerve recordings are also evident in proprioceptive circuits in the spinal cord. We used an ex vivo hemisected spinal cord preparation and measured properties of the monosynaptic reflex circuit in $Na_V1.6^{fl/fl}$, $Na_V1.6^{het}$, and $Na_V1.6^{cKO}$ mice (Fig. 4). We first analyzed responses from mice in early postnatal development (P6 to P11) as all prior work has used this age range for monosynaptic reflex analysis, largely due to technical challenges associated with increased myelination in the ventral horn as development proceeds (*19*). In stark contrast to our muscle-nerve recordings, monosynaptic responses were similar between genotypes at this time point (Fig. 4). We only observed a significant difference in response latency in $Na_V1.6^{cKO}$ hemicords compared to that in $Na_V1.6^{het}$ and $Na_V1.6^{fl/fl}$ hemicords (Fig. 4B). No other genotype-dependent differences were observed across quantified parameters (Fig. 4, C to F). These findings suggest that, during early postnatal development, $Na_V1.6$ is dispensable for proprioceptor synaptic transmission.

Previous studies indicate that proprioceptors are not transcriptionally mature until walking behaviors begin to emerge (*20*), which occurs around P13. Thus, we decided to test monosynaptic responses beyond this time point (P14 to P18). Notably, at this age, proprioceptive synaptic transmission is nearly lost in $Na_V1.6^{cKO}$ hemicords (Fig. 4G). We found highly significant genotype-dependent differences between $Na_V1.6^{cKO}$ and $Na_V1.6^{fl/fl}$ hemicords across all quantified parameters (Fig. 4, H to L). This suggests that, following the onset of walking behaviors, $Na_V1.6$ is essential for proprioceptor synaptic transmission onto alpha motor neurons, which is also consistent with data from ex vivo muscle nerve recordings in adult afferents (Figs. 2 and 3). In addition, we also found significantly increased monosynaptic reflex response latencies and thresholds (Fig. 4, H and J), as well as significantly reduced response amplitudes in $Na_V1.6^{het}$ hemicords compared to those in $Na_V1.6^{fl/fl}$ controls (Fig. 4I). Last, when looking within genotypes, we found that, unlike in $Na_V1.6^{fl/fl}$ hemicords, which only showed a significant increase in response latency, there was a significant degradation of the monosynaptic reflex response in

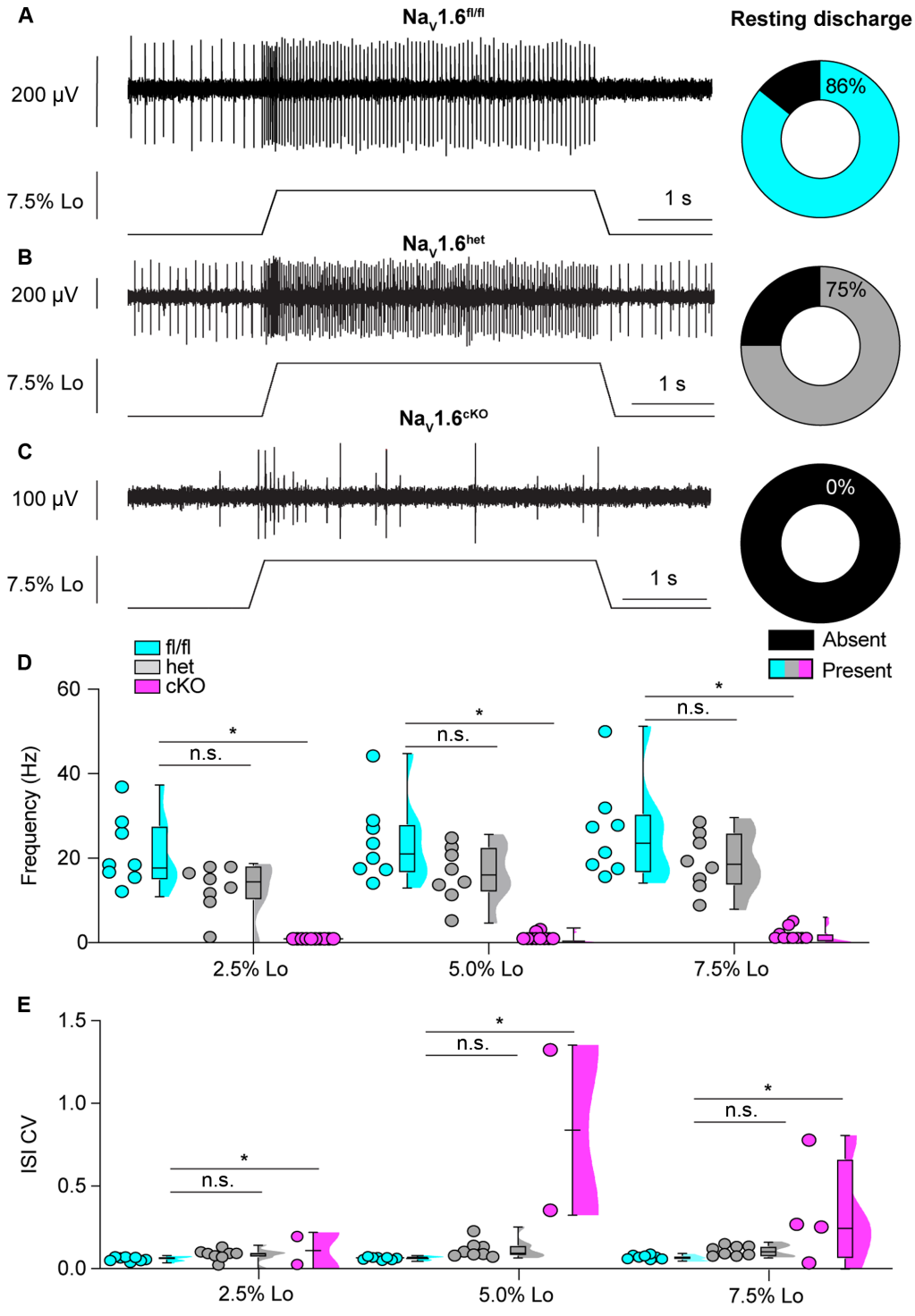

Fig. 2. Loss of Na$_V$1.6 abolishes muscle proprioceptor static stretch sensitivity. Representative responses to ramp-and-hold muscle stretch at 7.5% of optimal length (Lo) in Na$_V$1.6$^{fl/fl}$ (**A**), Na$_V$1.6^{het} (**B**), and Na$_V$1.6^{cKO} (**C**) muscle proprioceptors. The percentage of afferents that displayed resting discharge at Lo are represented by the pie charts to the right (black indicates absence of resting discharge). (**D**) Quantification of afferent firing frequency 3.25 to 3.75 s into stretch protocol. Na$_V$1.6$^{fl/fl}$ (cyan), Na$_V$1.6^{het} (gray), and Na$_V$1.6^{cKO} (magenta). Na$_V$1.6^{het} ($P = 0.178$) and Na$_V$1.6^{cKO} ($P = 0.001$) compared to Na$_V$1.6$^{fl/fl}$. (**E**) Firing regularity was quantified as the coefficient of variation of the interspike interval (ISI CV) of 1.5 to 3.5 s into the stretch protocol. Na$_V$1.6^{het} ($P = 0.669$) and Na$_V$1.6^{cKO} ($P = 0.000$) compared to Na$_V$1.6$^{fl/fl}$. In 6 of the 10 animals, we observed no response to stretch and therefore could only include the quantifiable responses from four afferents from Na$_V$1.6^{cKO} mice. Only quantifiable responses were included in statistical analyses in (D) and (E). Box and whisker plots represent maximum, minimum, median, and upper and lower quartiles of datasets. Each dot represents a single afferent. A two-way mixed-design ANOVA (Dunnett's post hoc comparison) was used to determine statistical significance in (D) and (E). Na$_V$1.6$^{fl/fl}$, $n = 8$ and $N = 7$; Na$_V$1.6^{het}, $n = 8$ and $N = 8$; and Na$_V$1.6^{cKO}, $n = 4$ and $N = 10$. n = afferents and N = mice.

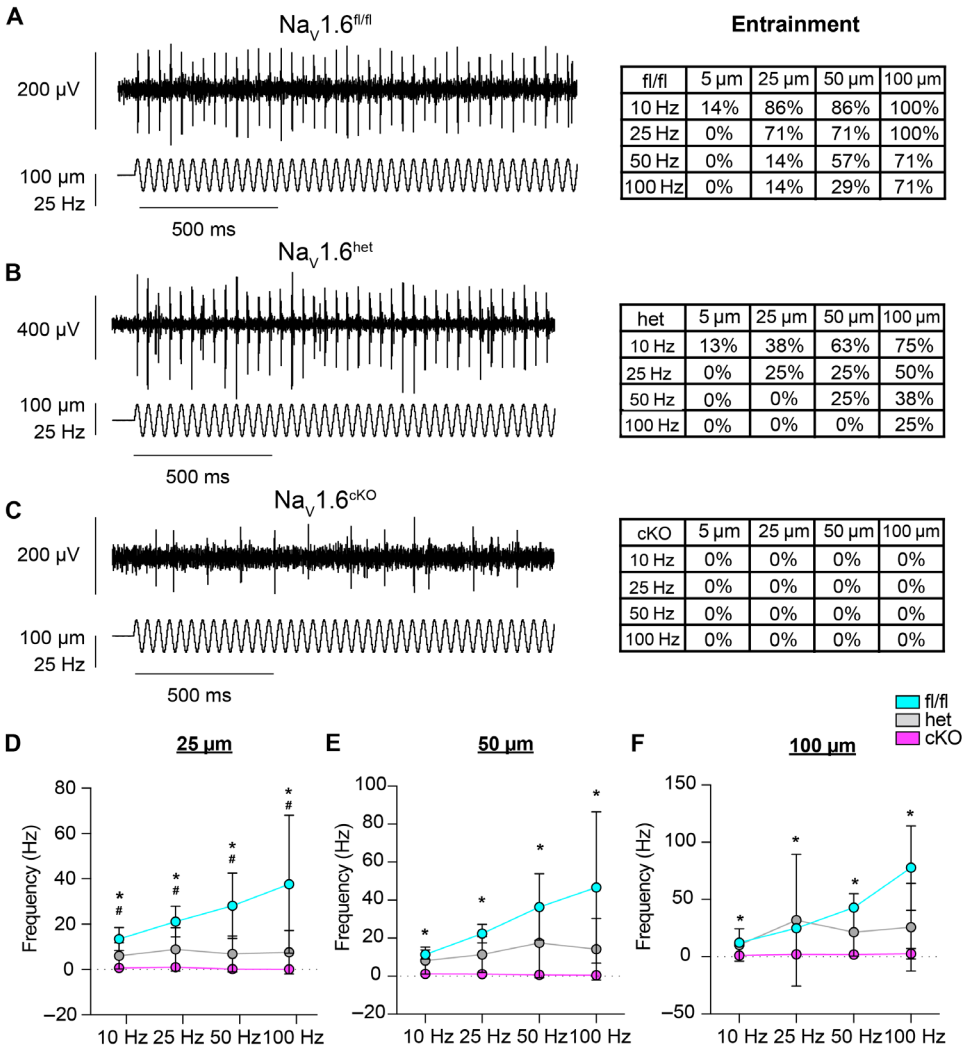

Fig. 3. Na$_V$1.6 is required for proprioceptor responses to vibration. Representative traces from Na$_V$1.6$^{fl/fl}$ (**A**), Na$_V$1.6^{het} (**B**), and Na$_V$1.6^{cKO} (**C**) afferents that were able to entrain to a 25-Hz, 100-µm amplitude vibration stimulus. Tables to the right indicate the percentage of afferents that were able to entrain across stimulus frequencies and amplitudes (Na$_V$1.6$^{fl/fl}$, top; Na$_V$1.6^{het}, middle; and Na$_V$1.6^{cKO}, bottom). (**D** to **F**) Quantification of firing frequency across vibration amplitudes. At 25 µm (D), Na$_V$1.6^{het} ($P = 0.005$) (# denotes significance in Na$_V$1.6^{het}) and Na$_V$1.6^{cKO} ($P = 0.001$) compared to Na$_V$1.6$^{fl/fl}$ (* denotes significance in Na$_V$1.6^{cKO}). At 50 µm (E), Na$_V$1.6^{het} ($P = 0.053$) and Na$_V$1.6^{cKO} ($P = 0.002$) compared to Na$_V$1.6$^{fl/fl}$. At 100 µm (F), Na$_V$1.6^{het} ($P = 0.414$) and Na$_V$1.6^{cKO} ($P = 0.018$) compared to Na$_V$1.6$^{fl/fl}$. Na$_V$1.6$^{fl/fl}$ (cyan), Na$_V$1.6^{het} (gray), and Na$_V$1.6^{cKO} (magenta). A two-way mixed-design ANOVA (Dunnett's post hoc comparison) was used to determine statistical in (D) to (F). Box and whisker plots represent maximum, minimum, median, and upper and lower quartiles of datasets. Each dot represents the average afferent response per genotype. Na$_V$1.6$^{fl/fl}$, $n = 8$ and $N = 7$; Na$_V$1.6^{het}, $n = 8$ and $N = 8$; and Na$_V$1.6^{cKO}, $n = 4$ and $N = 10$. n = afferents and N = mice.

Na$_V$1.6^{het} and Na$_V$1.6^{cKO} hemicords (table S1). Thus, during postnatal development, Na$_V$1.6$^{fl/fl}$ animals exhibit an enhancement in central proprioceptive signaling, whereas, in both Na$_V$1.6^{het} and Na$_V$1.6^{cKO} mice, central proprioceptive signaling degrades. This provides additional evidence that, at the circuit level, Na$_V$1.6 is haploinsufficient for proprioceptor synaptic function.

The developmental dependence of the proprioceptor-mediated monosynaptic reflex response on Na$_V$1.6 prompted us to investigate motor behaviors in this line at P7 and P14, before and after the onset of weight-bearing locomotion, respectively. We analyzed P7 mice in a righting reflex assay, a hindlimb suspension test, a grasping reflex assay, and quantified hindlimb angle. In line with spinal cord electrophysiology data, behavioral testing at P7 found a minimal role of Na$_V$1.6 across behavioral assays (fig. S2, A to H); we only observed a significant difference in hindlimb angle at this age. Conversely, when we analyzed motor abilities in a limb coordination assay at P14, we observed significant differences in functional grasping in both Na$_V$1.6^{het} and Na$_V$1.6^{cKO} mice compared to that in Na$_V$1.6$^{fl/fl}$ controls (fig. S2, I to J). These data highlight a developmentally specific contribution of Na$_V$1.6 to proprioceptive synaptic transmission in the spinal cord, which also manifests at the behavioral level.

Because we did not observe a role for Na$_V$1.6 in the proprioceptor-mediated monosynaptic reflex response between P6 and P11, we next asked whether instead Na$_V$1.1 was required for proprioceptor synaptic transmission at this developmental stage. In line with our findings across Na$_V$1.6 genotypes, monosynaptic reflex responses were genotype-independent in the Na$_V$1.1 mouse line in this age range (Fig. 5). These data suggest that proprioceptor synaptic

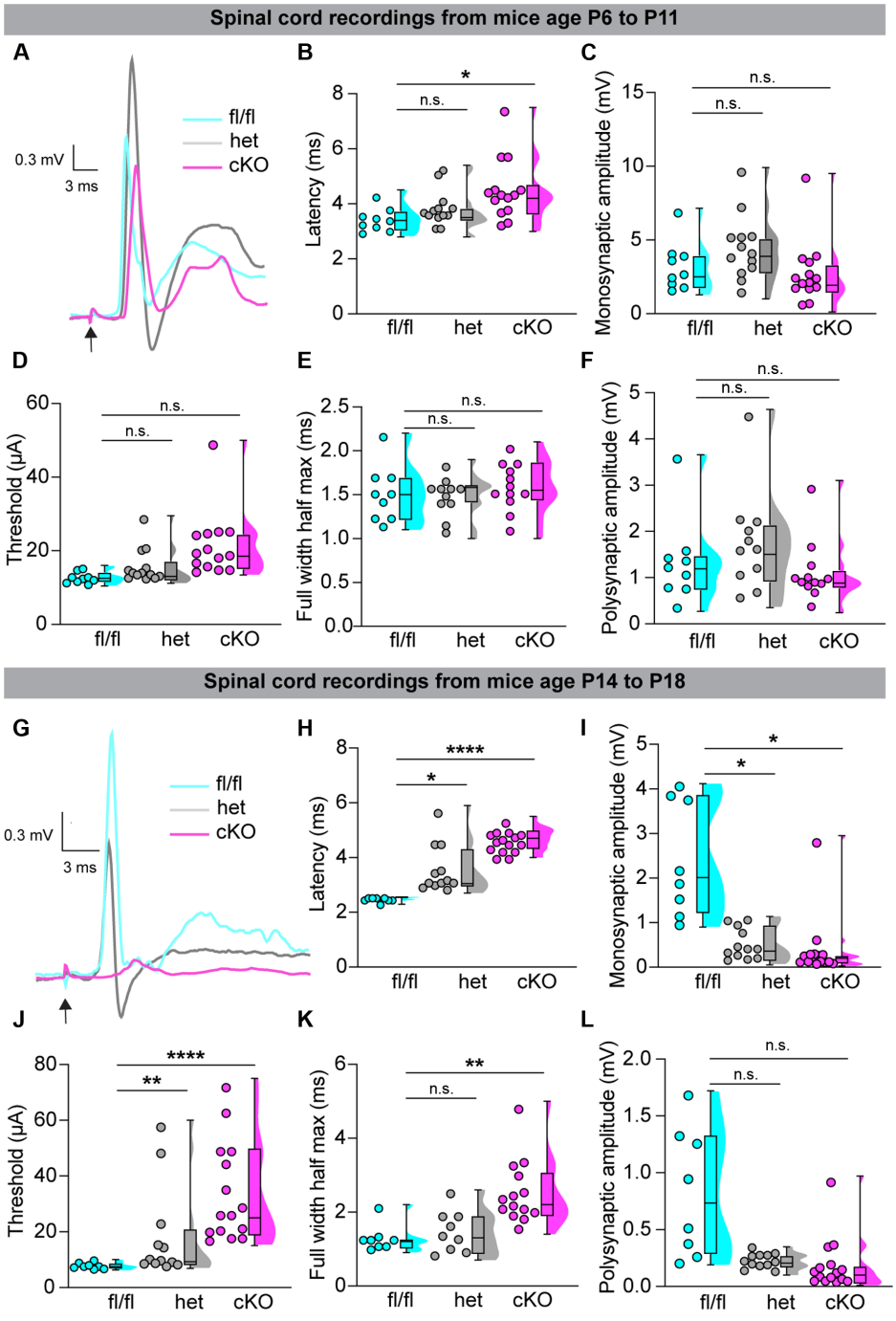

Fig. 4. $Na_V1.6$ plays a developmentally dependent role in proprioceptor synaptic transmission in the spinal cord. (**A**) Representative monosynaptic reflex responses from $Na_V1.6^{fl/fl}$ (cyan), $Na_V1.6^{het}$ (gray), and $Na_V1.6^{cKO}$ (magenta) hemicords during P6 to P11. Quantification of response properties. (**B**) Response latency, $Na_V1.6^{het}$ ($P = 0.760$) and $Na_V1.6^{cKO}$ ($P = 0.019$) compared to $Na_V1.6^{fl/fl}$. (**C**) Monosynaptic response amplitude, $Na_V1.6^{het}$ ($P = 0.238$) and $Na_V1.6^{cKO}$ ($P = 0.640$) compared to $Na_V1.6^{fl/fl}$. (**D**) Stimulus threshold, $Na_V1.6^{het}$ ($P = 0.910$) and $Na_V1.6^{cKO}$ ($P = 0.271$) compared to $Na_V1.6^{fl/fl}$. (**E**) Full width half maximum, $Na_V1.6^{het}$ ($P = 0.999$) and $Na_V1.6^{cKO}$ ($P = 0.929$) compared to $Na_V1.6^{fl/fl}$. (**F**) Polysynaptic response amplitude, $Na_V1.6^{het}$ ($P = 0.514$) and $Na_V1.6^{cKO}$ ($P = 0.704$) compared to $Na_V1.6^{fl/fl}$. (**G**) Representative monosynaptic reflex responses in $Na_V1.6^{fl/fl}$ (cyan), $Na_V1.6^{het}$ (gray), and $Na_V1.6^{cKO}$ (magenta) hemicords during P14 to P18. (**H**) Response latency, $Na_V1.6^{het}$ ($P = 0.023$) and $Na_V1.6^{cKO}$ ($P < 0.0001$) compared to $Na_V1.6^{fl/fl}$. (**I**) Monosynaptic response amplitude, $Na_V1.6^{het}$ ($P = 0.037$) and $Na_V1.6^{cKO}$ ($P = 0.018$) compared to $Na_V1.6^{fl/fl}$. (**J**) Stimulus threshold, $Na_V1.6^{het}$ ($P = 0.164$) and $Na_V1.6^{cKO}$ ($P < 0.0001$) compared to $Na_V1.6^{fl/fl}$. (**K**) Full width half maximum, $Na_V1.6^{het}$ ($P = 0.784$) and $Na_V1.6^{cKO}$ ($P < 0.0001$) compared to $Na_V1.6^{fl/fl}$. (**L**) Polysynaptic response amplitude, $Na_V1.6^{het}$ ($P = 0.143$) and $Na_V1.6^{cKO}$ ($P = 0.092$) compared to $Na_V1.6^{fl/fl}$. Each dot represents a single hemicord. [(A) to (F)] $Na_V1.6^{fl/fl}$, $n = 9$; $Na_V1.6^{het}$, $n = 13$; and $Na_V1.6^{cKO}$, $n = 14$. [(G) to (L)] $Na_V1.6^{fl/fl}$, $n = 8$; $Na_V1.6^{het}$, $n = 12$; and $Na_V1.6^{cKO}$, $n = 15$. $N = 8$ to 15. n = hemicords and N = mice. Box and whisker plots represent maximum, minimum, median, and upper and lower quartiles of datasets. A two-way mixed-design ANOVA (Tukey's post hoc comparison) was used to determine statistical significance.

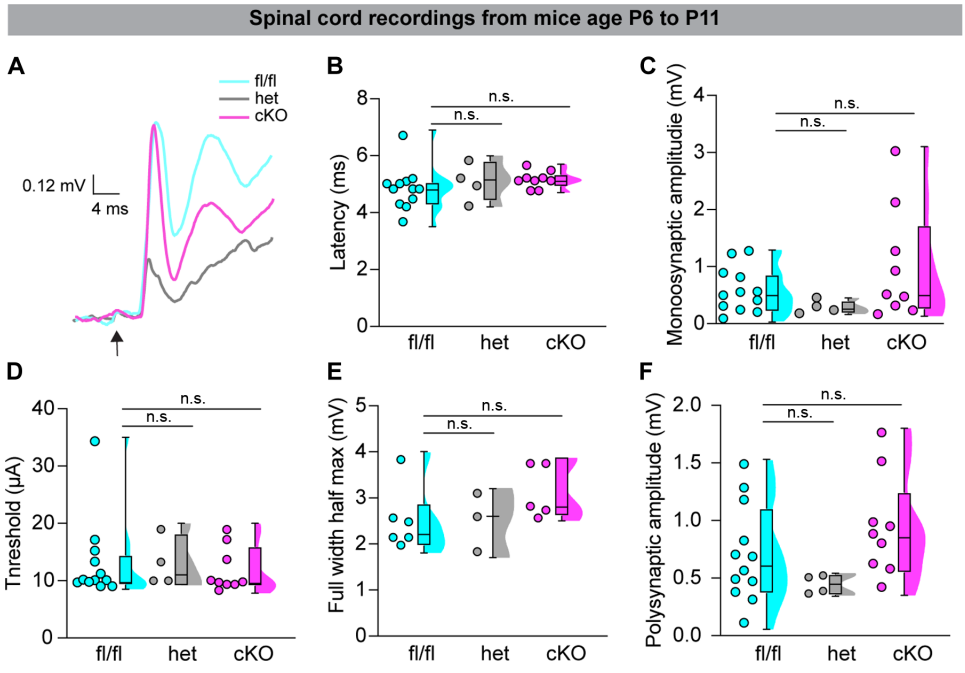

Fig. 5. $Na_V1.1$ does not contribute to proprioceptor synaptic transmission before the onset of walking behaviors. (**A**) Representative monosynaptic reflex responses from $Na_V1.1^{fl/fl}$ (cyan), $Na_V1.1^{het}$ (gray), and $Na_V1.1^{cKO}$ (magenta) hemicords recorded during P6 to P11. (**B** to **D**) Quantification of monosynaptic response properties. (B) Response latency, $Na_V1.1^{het}$ ($P = 0.723$) and $Na_V1.1^{cKO}$ ($P = 0.238$) compared to $Na_V1.1^{fl/fl}$. (C) Monosynaptic response amplitude, $Na_V1.1^{het}$ ($P = 0.378$) and $Na_V1.1^{cKO}$ ($P > 0.999$) compared to $Na_V1.1^{fl/fl}$. (D) Stimulus threshold, $Na_V1.1^{het}$ ($P > 0.999$) and $Na_V1.1^{cKO}$ ($P > 0.999$) compared to $Na_V1.1^{fl/fl}$. (**E**) Full width half maximum, $Na_V1.1^{het}$ ($P > 0.999$) and $Na_V1.1^{cKO}$ ($P = 0.255$) compared to $Na_V1.1^{fl/fl}$. (**F**) Polysynaptic response amplitude, $Na_V1.1^{het}$ ($P = 0.574$) and $Na_V1.1^{cKO}$ ($P = 0.473$) compared to $Na_V1.1^{fl/fl}$. Each dot represents a single hemicord. $Na_V1.1^{fl/fl}$, $n = 12$; $Na_V1.1^{het}$, $n = 4$; and $Na_V1.1^{cKO}$, $n = 9$. $N = 4$ to 10 mice. Box and whisker plots represent maximum, minimum, median, and upper and lower quartiles of datasets. A Kruskal-Wallis test with Dunn's multiple comparisons was used to determine statistical significance.

transmission at early postnatal development is not dependent on $Na_V1.1$ or $Na_V1.6$ and could indicate Na_V functional redundancy in proprioceptors before the onset of walking behaviors. We attempted to measure the monosynaptic reflex in later postnatal development (P14 to P18) in these mice; however, responses across all genotypes were too small to reliably quantify, despite our ability to obtain recordings at this age from mice in the Nav1.6 line (Fig. 4) as well as age-matched C57Bl/6J controls (fig. S3). Thus, we cannot rule out the possibility that $Na_V1.1$ may serve a role in proprioceptor-mediated synaptic transmission following the acquisition of weight-bearing locomotion. Behavioral testing at P7 did not reveal changes in motor function across genotypes (fig. S4, A and B). At P14, however, we did observe a significant difference in functional grasping in $Na_V1.1^{cKO}$ mice compared to that in $Na_V1.1^{fl/fl}$ controls (fig. S4E), suggesting that $Na_V1.1$ also becomes important for motor coordination at the onset of walking behaviors. These data show that, in early postnatal development neither $Na_V1.1$ nor $Na_V1.6$ alone is required for proprioceptor synaptic transmission; however, upon the acquisition of weight-bearing locomotion, we find that $Na_V1.6$ becomes functionally dominant at the circuit level, and both $Na_V1.1$ and $Na_V1.6$ are required at the behavioral level.

Severely, but not moderately, impaired proprioception results in deficits in muscle spindle development

A recent study found that loss of Piezo2 or $Na_V1.6$ in sensory neurons led to changes in tactile sensory neuron end organ development (*21*). This study raised the possibility that $Na_V1.6$ may also regulate muscle spindle development. As with our prior examination of $Na_V1.1^{cKO}$ mice compared to controls, we did not observe a reduction in the overall number of proprioceptors in DRG sections (identified by *Pvalb* and *Runx3* colocalization) between $Na_V1.6^{fl/fl}$, $Na_V1.6^{het}$, and $Na_V1.6^{cKO}$ mice (fig. S5B). We next examined the structure of muscle spindles in $Na_V1.6^{cKO}$ mice by performing immunohistochemistry against vesicular glutamate transporter 1 (VGLUT1) to visualize muscle spindle sensory wrappings in sections of extensor digitorum longus (EDL) muscle. Qualitative observation of muscle spindles from $Na_V1.6^{cKO}$ mice shows notable structural abnormalities in sensory wrappings that were not present in $Na_V1.6^{fl/fl}$ or $Na_V1.6^{het}$ animals (Fig. 6, A to C). To our knowledge, there is no standardized method to quantitatively assess the structure of muscle spindles. Thus, we devised a quantitative method to examine muscle spindle sensory terminals by measuring the colocalization of $VGLUT1^+$ sensory wrappings around clusters of 4′,6-diamidino-2-phenylindole (DAPI)–positive nuclei, which represent intrafusal muscle fibers. By normalizing the number of wrappings to muscle spindle length, we calculated a wrapping efficiency index (WEI). We found that, compared to those from $Na_V1.6^{fl/fl}$ and $Na_V1.6^{het}$ animals, muscle spindles from $Na_V1.6^{cKO}$ mice had significantly reduced wrapping efficiency indices, demonstrating that $Na_V1.6$ in sensory neurons is required for muscle spindle development (Fig. 6D). To validate that the structural changes that we observed were not due disruptions in VGLUT1 expression, we repeated these experiments using the pan-neuronal marker βIII-tubulin. Both antibodies revealed a significant reduction in WEI in $Na_V1.6^{cKO}$ muscle spindles compared to that in floxed controls (fig. S6). In our prior work, we qualitatively reported that loss of $Na_V1.1$ does not change muscle spindle structure (*7*). To confirm our

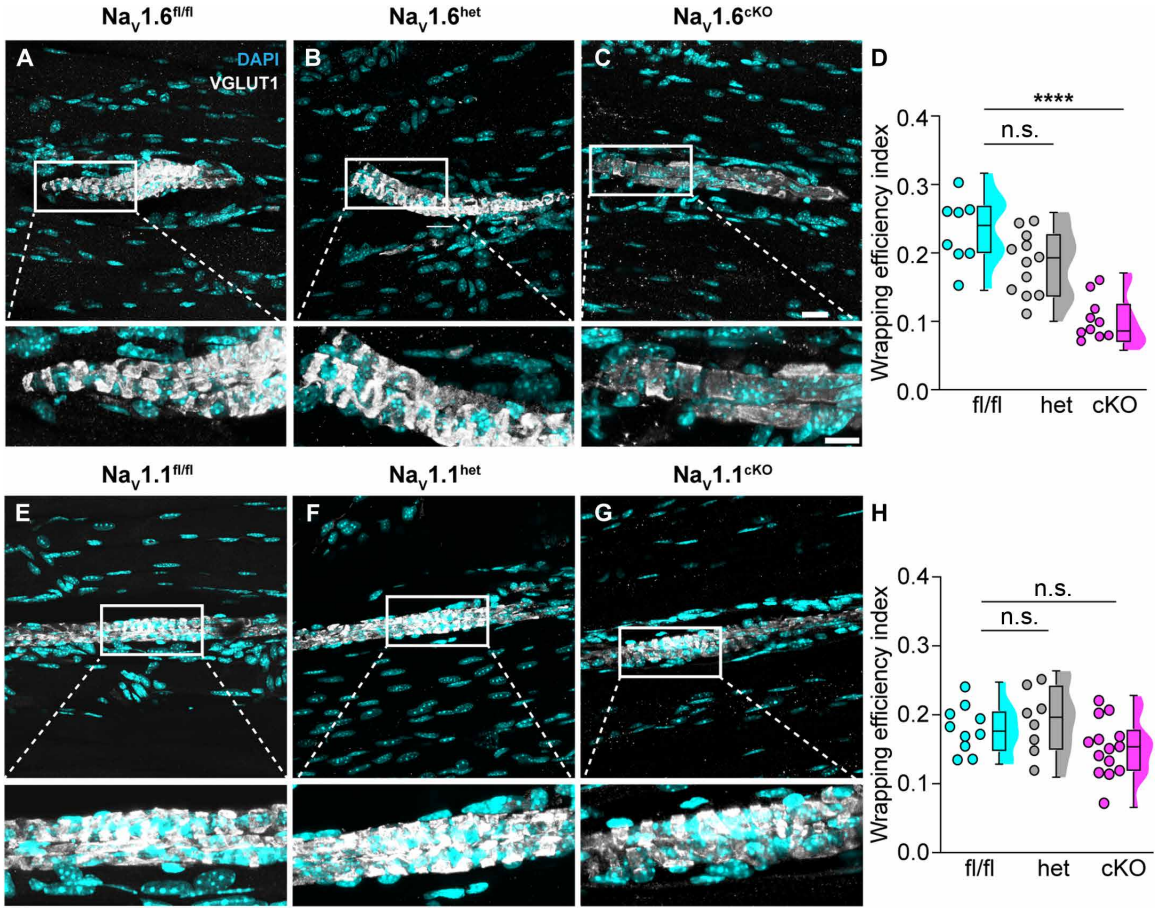

Fig. 6. Loss of Na$_V$1.6, but not Na$_V$1.1, in somatosensory neurons impairs muscle spindle development. Representative confocal images of muscle spindles from (**A**) Na$_V$1.6$^{fl/fl}$, (**B**) Na$_V$1.6^{het}, and (**C**) Na$_V$1.6^{cKO} extensor digitorum longus (EDL) muscle sections (30 μm). Images were acquired with a 60× oil 1.4 numerical aperture (NA) lens. VGLUT1 (gray scale) labels proprioceptor sensory terminals, and 4′,6-diamidino-2-phenylindole (DAPI; cyan) labels nuclei. Insets below images show the colocalization of sensory terminals with DAPI. (**D**) Quantification of wrapping efficiency index (WEI) based on colocalization of DAPI with VGLUT1. Na$_V$1.6^{het} ($P = 0.0658$) and Na$_V$1.6^{cKO} ($P < 0.0001$) compared to Na$_V$1.6$^{fl/fl}$. Representative images of muscle spindles from (**E**) Na$_V$1.1$^{fl/fl}$, (**F**) Na$_V$1.1^{het}, and (**G**) Na$_V$1.1^{cKO}. (**H**) Quantification of WEI based on colocalization of DAPI with VGLUT1. Na$_V$1.1^{het} ($P = 0.762$) and Na$_V$1.1^{cKO} ($P = 0.282$) compared to Na$_V$1.1$^{fl/fl}$. Each dot represents a single muscle spindle section. (D) Na$_V$1.6$^{fl/fl}$, $n = 8$; Na$_V$1.6^{het}, $n = 12$; and Na$_V$1.6^{cKO}, $n = 10$. (H) Na$_V$1.1$^{fl/fl}$, $n = 10$; Na$_V$1.1^{het}, $n = 8$; and Na$_V$1.1^{cKO}, $n = 14$. $N = 3$ mice per genotype. Box and whisker plots represent maximum, minimum, median, and upper and lower quartiles of datasets. A one-way ANOVA (Dunnett's post hoc comparison) was used to determine statistical significance. Scale bar, 20 μm. Inset scale bar, 10 μm.

previous findings using this quantitative approach, we analyzed the WEI of muscle spindles from Na$_V$1.1^{cKO} mice compared to those from Na$_V$1.1^{het} and Na$_V$1.1$^{fl/fl}$ controls (Fig. 6, E to H). In line with our previous work, Na$_V$1.1 is not required for muscle spindle development as wrapping efficiency indices were not significantly different between genotypes (Fig. 6H). Thus, the above results show that muscle spindle development is impaired when proprioceptive signaling is severely, but not moderately, disrupted.

Proprioceptive feedback is required for normal skeletal muscle development

Global inactivation of Na$_V$1.6 leads to severe motor impairments accompanied by atrophy of skeletal muscle (*22*). It was hypothesized that these deficits were caused by loss of signal transmission from motor neurons; however, whether impaired proprioceptive feedback onto motor neurons is sufficient to impair skeletal muscle development has not been directly investigated. To address this, we analyzed skeletal muscle anatomy and function in the Na$_V$1.6 mouse line. We collected soleus muscle from mice and labeled for slow (type I) and fast (type IIa) twitch muscle fibers. Muscle fibers from Na$_V$1.6^{cKO} mice had a visible reduction in muscle fiber size compared to fibers from Na$_V$1.6^{het} and Na$_V$1.6$^{fl/fl}$ mice (Fig. 7, A to C). To quantify these changes, we took an unbiased approach and measured muscle fiber properties using a semiautomatic muscle fiber analysis software in MATLAB (*23*). In agreement with qualitative observation, muscle fibers from Na$_V$1.6^{cKO} mice displayed a significant decrease in fiber area compared to Na$_V$1.6^{het} and Na$_V$1.6$^{fl/fl}$ muscle (Fig. 7D). A cumulative distribution plot shows the spread of muscle fiber area across genotypes (Fig. 7E). The proportion of type I and type IIa fibers was also similar between genotypes and was within the expected percentages for soleus muscle in wild-type animals (fig. S7, A and B) (*24*, *25*). Furthermore, we found that the size of both type I and type IIa fibers in Na$_V$1.6^{cKO} mice was significantly reduced compared to other that of genotypes, indicating the changes in muscle fiber area were not fiber-type specific (fig. S7, C and D). We next examined whether the developmental changes in

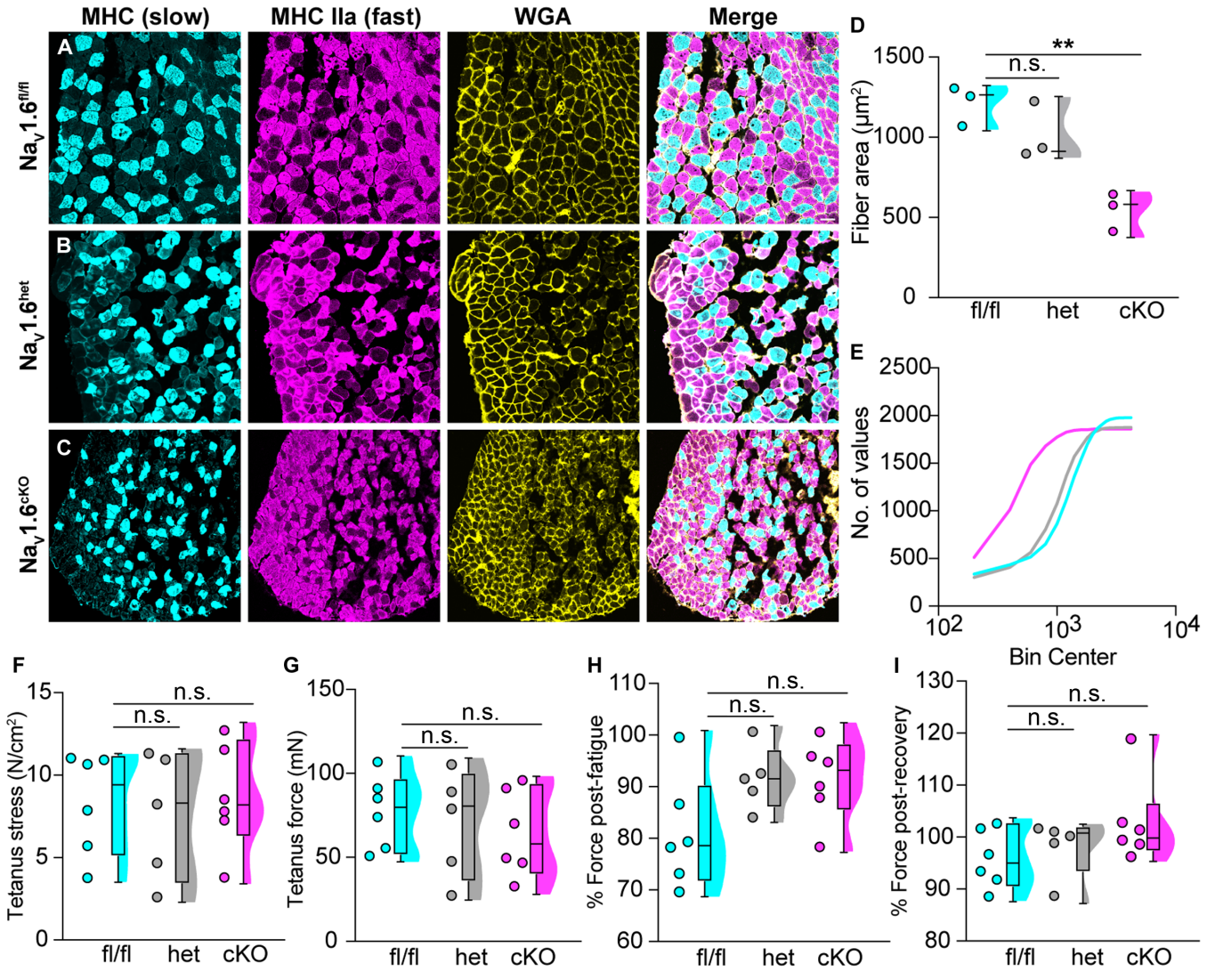

Fig. 7. Loss of proprioceptive feedback alters skeletal muscle development in Na$_V$1.6^{cKO} mice. Representative images of muscle fibers from the soleus of (**A**) Na$_V$1.6$^{fl/fl}$, (**B**) Na$_V$1.6^{het}, and (**C**) Na$_V$1.6^{cKO} mice. Images were acquired with a 20× 0.75 NA air lens. Myosin heavy chain (MHC) labels slow twitch muscle fibers (cyan), MHC type IIa labels fast twitch muscle fibers (magenta), and wheat germ agglutinin (WGA; yellow) labels the cell membrane of muscle fibers. (**D** and **E**) Quantification of muscle fiber anatomy. (D) Fiber area, Na$_V$1.6^{het} ($P = 0.337$) and Na$_V$1.6^{cKO} ($P = 0.006$) compared to Na$_V$1.6$^{fl/fl}$. (E) cumulative distribution plots showing the muscle fiber area in the soleus between Na$_V$1.6$^{fl/fl}$ (cyan), Na$_V$1.6^{het} (gray), and Na$_V$1.6^{cKO} (magenta) mice. (**F** to **I**) Quantification of intrinsic properties of soleus muscle. (F) Tetanus stress, Na$_V$1.6^{het} ($P = 0.926$) and Na$_V$1.6^{cKO} ($P = 0.990$) compared to Na$_V$1.6$^{fl/fl}$. (G) Tetanus force, Na$_V$1.6^{het} ($P = 0.925$) and Na$_V$1.6^{cKO} ($P = 0.690$) compared to Na$_V$1.6$^{fl/fl}$. (H) Percentage of force after fatigue, Na$_V$1.6^{het} ($P = 0.189$) and Na$_V$1.6^{cKO} ($P = 0.150$) compared to Na$_V$1.6$^{fl/fl}$. (I) Percentage of force after recovery, Na$_V$1.6^{het} ($P = 0.851$) and Na$_V$1.6^{cKO} ($P = 0.293$) compared to Na$_V$1.6$^{fl/fl}$. Each dot represents a single animal. Box and whisker plots represent maximum, minimum, median, and upper and lower quartiles of datasets. A one-way ANOVA (Dunnett's post hoc comparison) was used to determine statistical significance. Scale bar, 50 µm.

muscle fiber properties corresponded to alterations in intrinsic muscle strength and fatiguability; however, we found no differences in muscle function across genotypes (Fig. 7, F to I). Collectively, these reveal a non–cell-autonomous role for proprioceptive feedback in skeletal muscle development.

We next asked whether moderately impaired proprioceptive signaling due to loss of Na$_V$1.1 had the same effect on skeletal muscle development or function. We examined muscle fiber composition of Na$_V$1.1 mice of all genotypes and did not observe any significant changes in fiber area (Fig. 8, A to E). In addition, the proportion of type I and type IIa fibers was similar between genotypes (fig. S7 E and F). Functional analysis of intrinsic muscle properties in the soleus of Na$_V$1.1^{cKO} mice did not differ compared to that of Na$_V$1.1^{het} or Na$_V$1.1$^{fl/fl}$ mice (Fig. 8, F to I), suggesting that moderately impaired proprioceptive feedback does not result in deficits in skeletal muscle at the anatomical or functional levels. Together, these experiments unveil a role for proprioceptive feedback in skeletal muscle development.

Na$_V$1.1 and Na$_V$1.6 occupy distinct cellular domains within muscle spindles

Our results demonstrate that Na$_V$1.1 and Na$_V$1.6 have differential roles in proprioceptive signaling. We next sought out to define the

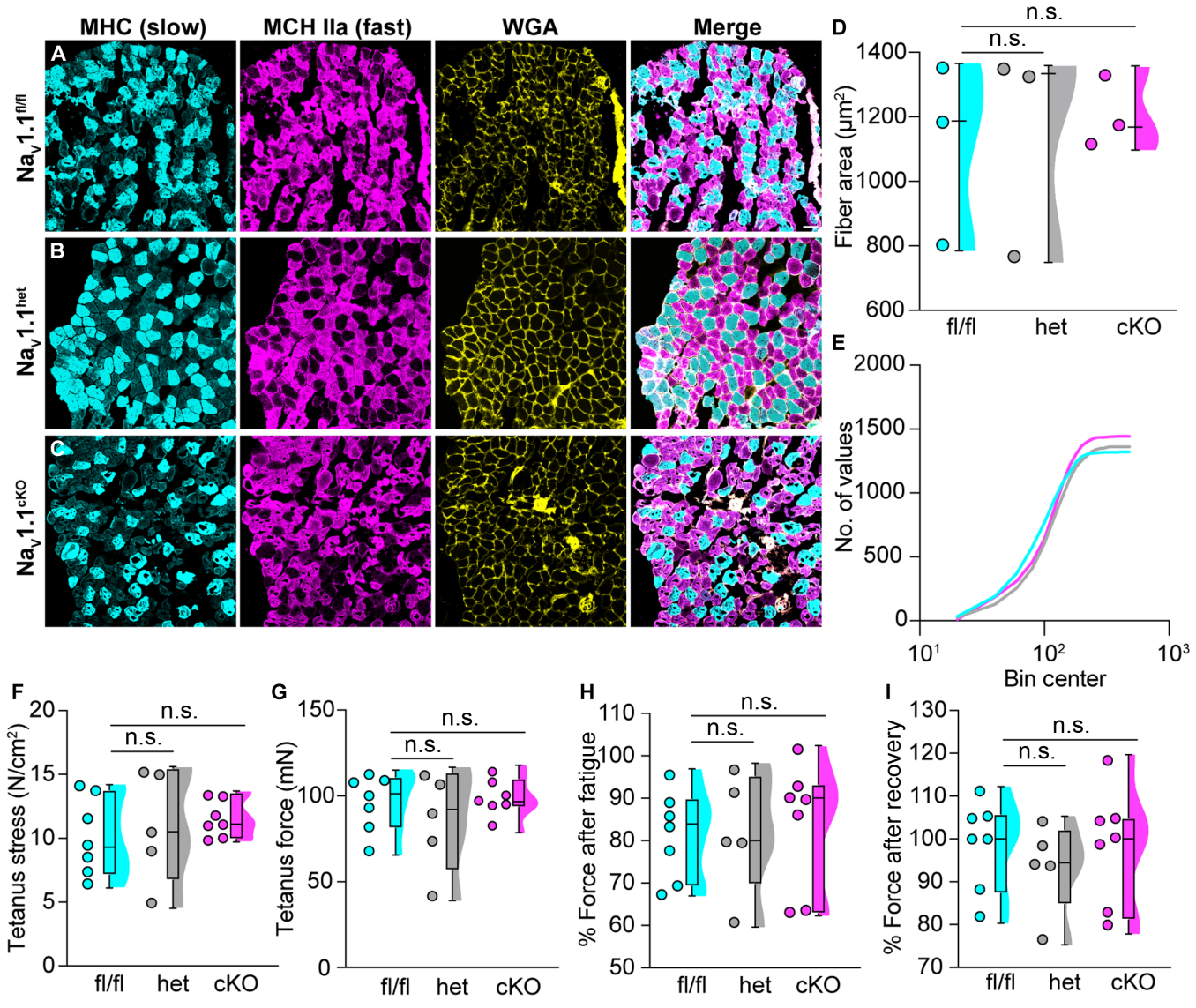

Fig. 8. Mildly impaired proprioceptive feedback does not impair skeletal muscle development. Images of muscle fibers from (**A**) $Na_V1.1^{fl/fl}$, (**B**) $Na_V1.1^{het}$, and (**C**) $Na_V1.6^{cKO}$ soleus muscle. Images were acquired with a 20× 0.75 NA air lens. MHC labels slow twitch muscle fibers (cyan), MHC type IIa labels fast twitch muscle fibers (magenta), and WGA (yellow) labels the cell membrane of muscle fibers. (**D** and **E**) Quantification of muscle fiber anatomy. (D) Fiber area, $Na_V1.1^{het}$ ($P = 0.9827$) and $Na_V1.1^{cKO}$ ($P = 0.880$) compared to $Na_V1.1^{fl/fl}$. (E) cumulative distribution plots showing the muscle fiber area between $Na_V1.1^{fl/fl}$ (cyan), $Na_V1.1^{het}$ (gray), and $Na_V1.1^{cKO}$ (magenta). (**F** to **I**) Quantification of intrinsic properties of soleus muscle. (F) Tetanus stress, $Na_V1.1^{het}$ ($P = 0.841$) and $Na_V1.1^{cKO}$ ($P = 0.596$) compared to $Na_V1.1^{fl/fl}$. (G) Tetanus force, $Na_V1.1^{het}$ ($P = 0.624$) and $Na_V1.1^{cKO}$ ($P = 0.978$) compared to $Na_V1.1^{fl/fl}$. (H) Percentage of force after fatigue, $Na_V1.1^{het}$ ($P = 0.999$) and $Na_V1.1^{cKO}$ ($P = 0.934$) compared to $Na_V1.1^{fl/fl}$. (I) Percentage of force after recovery, $Na_V1.1^{het}$ ($P = 0.724$) and $Na_V1.1^{cKO}$ ($P = 0.993$) compared to $Na_V1.1^{fl/fl}$. Each dot represents a single animal. Box and whisker plots represent maximum, minimum, median, and upper and lower quartiles of datasets. A one-way ANOVA (Dunnett's post hoc comparison) was used to determine statistical significance. Scale bar, 50 μm.

mechanistic basis of their distinct and nonredundant contributions. At the biophysical level, $Na_V1.1$ and $Na_V1.6$ are functionally very similar, and both contribute to peak, persistent, and resurgent sodium currents (*26*–*28*). Previous studies examining central neurons, however, show that $Na_V1.1$ and $Na_V1.6$ occupy distinct excitable domains (*29*–*31*), suggesting that differences in cellular localization could dictate the unique roles that these channels play in proprioception. Compared to the central nervous system, our understanding of Na_V expression in sensory terminals is extremely poor. We therefore set out to examine the expression patterns of $Na_V1.1$ and $Na_V1.6$ in proprioceptive end organs. We focused our analysis on muscle spindles, as these structures comprise two of the three proprioceptor functional classes (*1*) and are the afferent endings from which we recorded in ex vivo muscle nerve experiments (Figs. 2 and 3). We first labeled for $Na_V1.6$ channels and observed discrete, high-density clusters across the spindle that resembled action potential initiation zones (Fig. 9, A to C). We observed, on average, two $Na_V1.6^+$ clusters per muscle spindle section (Fig. 9D), although this is likely an underestimation of the total number of clusters per entire spindle. In central neurons, $Na_V1.6$ has been shown to play a major role in signal

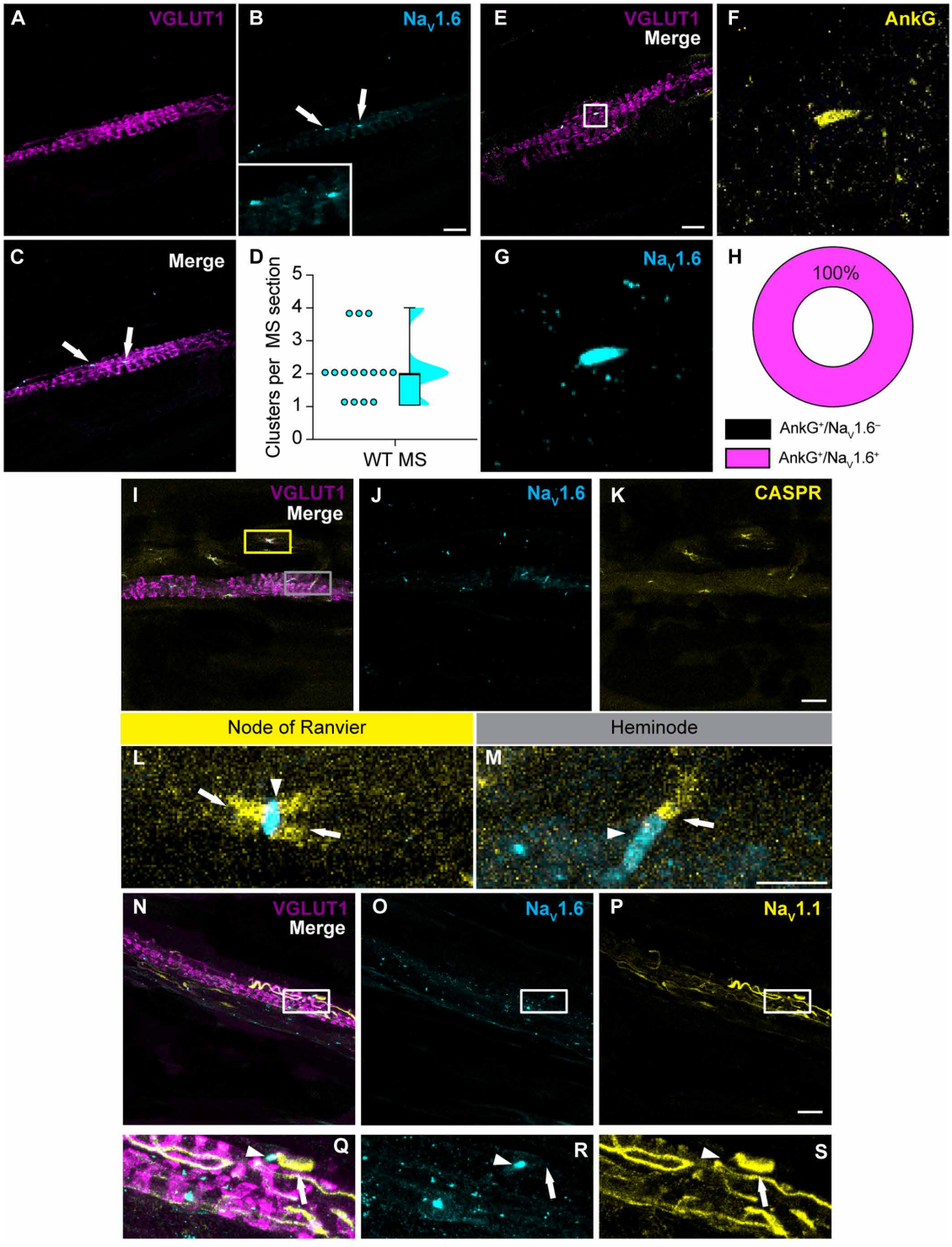

Fig. 9. Na$_V$1.1 and Na$_V$1.6 localize to discrete cellular regions in muscle spindles. VGLUT1 [magenta, (**A**)] labeled muscle spindles express clusters of Na$_V$1.6 [cyan, (**B** and **C**)]. Arrows denote clusters of Na$_V$1.6. (**D**) Quantification of the number of Na$_V$1.6 clusters per muscle spindle ($n = 15$ spindles). WT, wild type; MS, muscle spindle. (**E** to **H**) Na$_V$1.6 clusters (G) colocalize with Ankyrin-G [AnkG; yellow; (E) and (F) are insets from (G)]. (H) Quantification of the percentage of AnkG clusters that colocalize with Na$_V$1.6 clusters ($n = 9$ spindles). (**I** to **M**) Co-labeling of Na$_V$1.6 (J) with juxtaparanode maker CASPR [(K), yellow] reveal proprioceptor nodes of Ranvier (L) and heminodes (M) ($n = 10$ spindles). Nodes of Ranvier were identified by two CASPR$^+$ signals (arrows) flanking Na$_V$1.6 clusters (arrowheads). Heminodes were identified by a single CASPR$^+$ signals juxtaposed to Na$_V$1.6 cluster. (**N** to **S**) Co-labeling of Na$_V$1.6 (O) with Na$_V$1.1 [(P), yellow] shows discrete cellular expression patterns. [(Q) to (S)] Arrowheads denote Na$_V$1.6 channels, and arrows denote Na$_V$1.1 channels. $N = 3$ to 5 mice. Inset scale bars, 10 μm. Scale bars, 20 μm

initiation and propagation due to its expression at the distal axon initial segment (AIS) and nodes of Ranvier (*29*, *31*, *32*). Thus, we co-labeled with the AIS marker Ankyrin-G [AnkG; Fig. 9, E to G; (*33*)] and found that 100% of $Na_V1.6$ clusters colocalize with AnkG (Fig. 9H). To determine whether these clusters were bona fide heminodes or nodes of Ranvier, we co-labeled with the juxtaparanode marker CASPR (*34*). Triple immunolabeling experiments found $Na_V1.6$ clusters flanked by two $CASPR^+$ signals near $VGLUT1^+$ muscle spindles (Fig. 9, I to L), as well as in myelinated axons of the sciatic nerve (fig. S8). Furthermore, we also observed $Na_V1.6$ channel clusters flanked by a single $CASPR^+$ signal within muscle spindles, indicative of the presence of $Na_V1.6^+$ heminodes within muscle spindles (Fig. 9M). These findings reveal that $Na_V1.6$ is expressed only at heminodes within muscle spindles and nodes of Ranvier of proprioceptors, where it likely plays a direct role in signal initiation and propagation.

If $Na_V1.1$ and $Na_V1.6$ differentially regulate electrical signaling in proprioceptors through distinct cellular localization patterns, then co-labeling for both ion channels should reveal nonoverlapping expression patterns. In line with our hypothesis, we find a notable difference in $Na_V1.1$ localization in muscle spindles compared to $Na_V1.6$ (Fig. 9, N and Q). In contrast to the discrete clusters of $Na_V1.6$, we observe that $Na_V1.1$ localization is not clustered but restricted to more equatorial wrappings within muscle spindles and in some presumptive axons entering the muscle spindle (Fig. 9S). We ensured the specificity of $Na_V1.1$ and $Na_V1.6$ antibodies using tissue harvested from $Na_V1.1^{cKO}$ and $Na_V1.6^{cKO}$ mice, respectively (fig. S9).

Given that we found developmentally dependent roles for $Na_V1.1$ and $Na_V1.6$ in proprioceptor synaptic transmission in the spinal cord (Figs. 4 and 5), we asked whether Na_V localization is dynamic during postnatal development. We labeled for $Na_V1.1$ and $Na_V1.6$ in muscle spindles from the EDL of P7 and P14 C57Bl6/J mice (fig. S10) the time points at which we observed a change in the requirement for either channel to motor function (figs. S2 and S4). At P7, we observed no $Na_V1.6$ clusters within spindles, although we did find some clusters near spindles, which could represent nodes of Ranvier. At P14, clusters of $Na_V1.6$ begin to emerge within muscle spindles, although these clusters appear smaller and less frequently than those observed in adult muscle spindles. We detected little to no $Na_V1.1$ immunoreactivity in muscle spindles at P7 and P14, suggesting either no or low expression of this channel at these time points. Given the significant change in functional grasping observed in $Na_V1.1^{cKO}$ at P14 (fig. S4E), this would suggest that $Na_V1.1$ may serve a role in sensory transmission outside of the muscle spindle at this time point in postnatal development. Thus, we propose that the unique localization patterns of $Na_V1.1$ and $Na_V1.6$, which are dynamically regulated during postnatal development, confer the unique contributions of each channel to electrical signaling in proprioceptors.

DISCUSSION

The discovery of Piezo2 shared the 2021 Nobel Prize in Physiology and Medicine due to its essential role in the function of various mechanosensory neurons. In proprioceptors, Piezo2 initiates muscle mechanotransduction signaling (*4*, *5*); however, the downstream ion channels responsible for transmitting proprioceptive information to central circuits have remained mysterious. In proprioceptors, the acid-sensing channels ASIC2 and ASIC3 modestly contribute to proprioceptive behaviors and muscle afferent excitability (*35*, *36*), and hyperpolarization-activated cyclic nucleotide-gated channels (*37*) and voltage-gated potassium channels of the K_V1 family may work together to set proprioceptor intrinsic excitability (*20*). Here, we demonstrate that Na_Vs differentially encode mammalian proprioception, and we predict this is largely due to differences in channel localization within proprioceptors (Fig. 10). Our prior work found that $Na_V1.1$ is essential for maintaining consistent and reliable proprioceptor encoding of static muscle stretch (*7*); this is consistent with its expression at sensory wrappings of muscle spindles where is it poised to integrate and amplify Piezo2-mediated mechanotransduction currents. Conversely, because of its localization at heminodes within muscle spindles and nodes of Ranvier, $Na_V1.6$ has an obligate role in initiating proprioceptor action potential firing. This is in line with ex vivo recordings from $Na_V1.6^{cKO}$ afferents, in which responses to both dynamic and static muscle movement are abolished (Figs. 2 and 3). Furthermore, this demonstrates that the activity of Piezo2 and other ion channels in proprioceptors cannot compensate for the loss of $Na_V1.6$. Thus, we conclude that $Na_V1.6$ is equally essential for mammalian proprioception as Piezo2. Taken together, this study investigates and defines unique and nonredundant roles for Na_Vs in encoding a specific somatosensory modality.

At the behavioral level, deletion of $Na_V1.1$ or $Na_V1.6$ in sensory neurons led to phenotypically distinct motor deficits. Previously, we reported that $Na_V1.1^{cKO}$ mice display uncontrollable intention-like tremors and poor motor coordination (*7*). Here, we show that deletion of $Na_V1.6$ in sensory neurons resulted in even more severe ataxia that precluded testing in the rotarod (Fig. 1). Notably, although more impaired than $Na_V1.1^{cKO}$ mice, $Na_V1.6^{cKO}$ mice did not display intention tremors. The distinct motor phenotypes that result from conditional deletion of $Na_V1.1$ or $Na_V1.6$ likely arise from differences in their respective contributions to proprioceptor function and development (Figs. 2, 3, and 6). In the open field, we found that the maximal speed of $Na_V1.6^{cKO}$ mice was significantly reduced compared to that of other genotypes (Fig. 1F). This finding is in line with prior work in $Egr3^{-/-}$ mice, in which muscle spindles do not develop, resulting in an inability of mice to walk at high speeds (*38*). It should be noted, however, that the behavioral phenotypes in these models cannot solely be attributed to proprioceptor dysfunction, as $Na_V1.1$ and $Na_V1.6$ are also expressed in tactile sensory neurons (*39*), which also contribute to motor behaviors (*40*, *41*). Nevertheless, at the afferent level, we show that $Na_V1.6$ is fundamentally essential for electrical signaling in proprioceptors, which contrasts the selective impairment on static stretch encoding observed in $Na_V1.1^{cKO}$ mice. Furthermore, $Na_V1.1$ deletion had no significant impact on muscle spindle or skeletal muscle development; therefore, it is likely that the deficits observed in $Na_V1.1^{cKO}$ are purely electrical in nature. By contrast, in addition to loss of proprioceptive transmission, $Na_V1.6^{cKO}$ mice had abnormal muscle spindle structure (Fig. 6) and significantly reduced skeletal muscle fiber size (Fig. 7), which suggests that the severe motor deficits in $Na_V1.6^{cKO}$ may be caused by both cell-autonomous and non–cell-autonomous mechanisms. Prior work on *Scn8a*^{med} mice show that global inactivation of $Na_V1.6$ resulted in a similar ataxic-like phenotype, as well as muscle atrophy and weakness (*12*, *22*). Our data show that loss of $Na_V1.6$ function in sensory neurons, particularly proprioceptors, is a major contributor to the motor and muscle impairments in *Scn8a*^{med} mice. This may have broader implications for interpreting the clinical manifestations associated with disease causing *Scn8a* mutations, which often result in motor dysfunction (*11*).

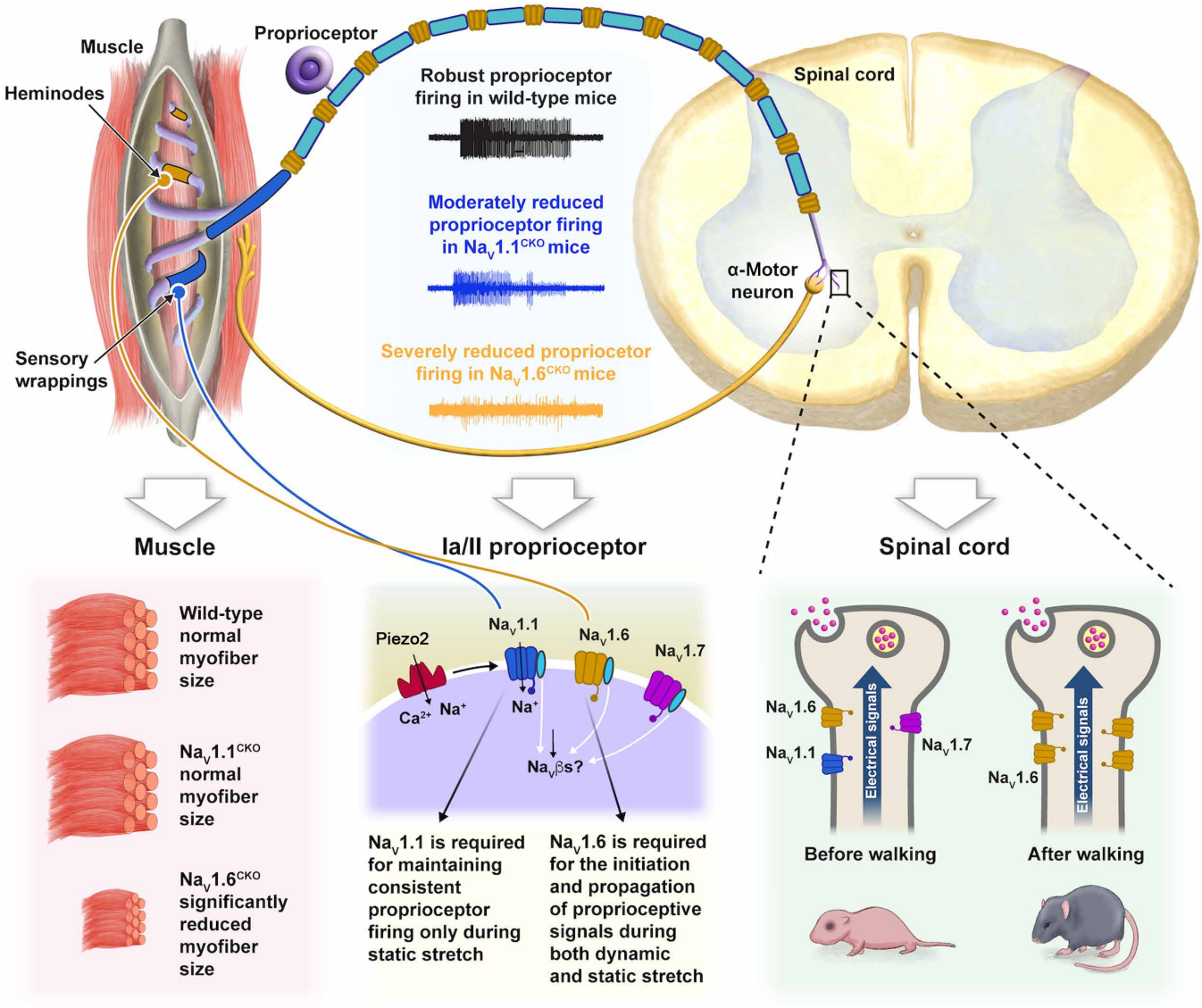

Fig. 10. Model of proprioceptive transmission by Na$_V$1.1 and Na$_V$1.6. Upon muscle stretch, Piezo2 (red) transduces mechanical stimuli into electrical potentials. Na$_V$1.1 (blue) expressed in muscle spindle sensory terminals integrates and amplifies Piezo2 signals to drive consistent proprioceptor firing during static muscle stretch. Na$_V$1.6 (yellow) localized to heminodes and nodes of Ranvier where it initiates and propagates proprioceptive signals from muscle spindles to the spinal cord. It is likely that before weight-bearing locomotion, there is functional redundancy of Na$_V$s in proprioceptive axons. After walking behaviors emerge, however, proprioceptive synaptic transmission is dependent on Na$_V$1.6. Deletion of Na$_V$1.6 in all sensory neurons led to a significant decrease in skeletal muscle fiber size that was not present in Na$_V$1.1^{cKO} muscle, suggesting that complete loss of proprioceptive feedback non–cell-autonomously regulates skeletal muscle development. Image credit: J. Tulman, UC Davis, Dept. of Physiology & Membrane Biology.

We found that a single copy of Na$_V$1.6 in sensory neurons was sufficient for normal motor function in adults (Fig. 1), despite being haploinsufficient in ex vivo muscle nerve recordings in response to vibration and in monosynaptic reflex recordings following the onset of walking behaviors (Figs. 3 and 4). In response to vibratory stimuli, afferents from Na$_V$1.6^{het} animals were less likely to entrain to sinusoidal vibration, particularly at 25-μm stimulus amplitudes (Fig. 3, B and D). Furthermore, in the spinal cord Na$_V$1.6^{het} animals displayed slower monosynaptic response latencies and required stronger current pulses to evoke a smaller amplitude response (Fig. 4, H to J). Why these functional deficits in Na$_V$1.6^{het} mice do not manifest at the behavioral level is unclear. It should be noted that, at P14, we observed Na$_V$1.6 haploinsufficiency in a limb coordination assay (fig. S2). It is therefore possible that compensatory mechanisms in Na$_V$1.6^{het} animals come into play in early adulthood. Another possibility is that Na$_V$1.6^{het} animals have more subtle motor deficits that were unresolvable in the open field and rotarod. More sensitive kinematic analyses with higher spatial and temporal resolution will be required to investigate the extent of Na$_V$1.6 haploinsufficiency for proprioceptor-driven motor behaviors.

We have very limited knowledge about the localization of ion channels within somatosensory end organs. This information is important for understanding how electrical signals arise within structurally complex sensory terminals, which can be damaged during

pathological conditions or aging (*1*, *42*–*44*). We show that $Na_V1.1$ and $Na_V1.6$ occupy distinct cellular compartments within proprioceptive muscle spindle end organs, which we predict underlies their differential roles in encoding proprioceptive signals. While differences in biophysical properties could also underlie the differential roles of $Na_V1.1$ and $Na_V1.6$ to proprioceptive transmission, these channels share many functional similarities. They both rapidly activate and inactivate; can generate peak, persistent, and resurgent currents; and have similar recovery from inactivation kinetics (*7*, *27*, *28*, *45*–*47*). Prior work in neurons of the central nervous system is consistent with our hypothesis that localization dictates Na_V contributions to proprioceptor function. For example, in retinal ganglion cells and motor neurons, $Na_V1.6$ is preferentially expressed at the distal AIS, suggesting a primary role in signal initiation (*48*, *49*). Furthermore, studies have shown that $Na_V1.6$ is the dominant isoform at nodes of Ranvier, playing a key role in action potential propagation in myelinated axons (*31*, *49*). In contrast, $Na_V1.1$ is localized to the soma and proximal AIS, where it aids in repetitive firing in fast spiking neurons of the brain (*14*, *50*). This is in line with our model whereby $Na_V1.1$ integrates and amplifies mechanotransduction currents from Piezo2 to maintain sustained action potential firing during static stretch.

We found that 100% of $Na_V1.6$ immunoreactivity colocalizes with AnkG. AnkG is known to anchor Na_Vs within the AIS of central neurons (*32*, *33*, *51*, *52*); thus, our findings indicate that muscle spindles have several $Na_V1.6$-expressing action potential initiation zones. Unexpectedly, we never observed broad AnkG immunoreactivity in muscle spindle sensory wrappings, indicating that AnkG does not colocalize with $Na_V1.1$, despite its known colocalization with $Na_V1.1$ at the AIS in other neurons of the central nervous system (*30*, *53*). The mechanisms that anchor $Na_V1.1$ to sensory terminals remain unknown. Scaffolding proteins known to colocalize with $Na_V1.1$ include βIV-spectrin, auxiliary $Na_V\beta$ subunits, and fibroblast growth factors (*14*, *54*, *55*). Proximity proteomic approaches could identify specific molecular players involved in $Na_V1.1$ channel organization within proprioceptive end organs.

Another unexpected result from our study was the developmentally dependent manner in which Na_Vs contribute to proprioceptor synaptic transmission in the spinal cord (Fig. 10). Ventral root recordings from mice at ages P6 to P11 revealed that neither $Na_V1.1$ nor $Na_V1.6$ is required for the proprioceptor-mediated monosynaptic reflex response at this age. Conversely, by P14, when proprioceptors are nearing molecular maturation and weight-bearing locomotion has emerged, $Na_V1.6$ becomes critical for this circuit. There are two principal interpretations for these data. First, before walking behaviors, neither $Na_V1.1$ nor $Na_V1.6$ contributes to proprioceptor synaptic transmission onto motor neurons. This interpretation would be consistent with previous studies in myelinated neurons of the retina, whereby the onset of eye opening corresponds with a developmental switch from $Na_V1.2$ to $Na_V1.6$ (*48*). It is possible that another Na_V subtype, such as $Na_V1.7$, is the dominant channel in early postnatal development. Alternatively, another interpretation is that, in early postnatal development, there is functional redundancy among Na_V subtypes, and loss of one is insufficient to impair synaptic transmission. This is line with a previous study that found the presence of multiple Na_V isoforms in sensory axons as early as P7 (*56*). We favor the latter interpretation because functional redundancy is a common phenomenon in the developing nervous system, and $Na_V1.7$ does not appear to play a substantial role in mammalian proprioception. Nevertheless, both interpretations indicate that the cellular trafficking mechanisms governing the stability of each Na_V subtype in this circuit are independent of one another, as loss of $Na_V1.6$ did not result in compensation by other Na_Vs following the onset of weight-bearing locomotion. Notably, our analyses of the monosynaptic reflex are consistent with behavioral analyses carried out in P7 and P14 mice, where motor function in P7 $Na_V1.1^{cKO}$ and $Na_V1.6^{cKO}$ mice was largely intact but declined by P14 (figs. S2 and S4). At P7, we observed little-to-no immunoreactivity of $Na_V1.1$ or $Na_V1.6$ in muscle spindles (fig. S9). By P14, $Na_V1.6$ clusters begin to appear within the spindle, while $Na_V1.1$ immunoreactivity remained weak. This suggests temporally distinct regulation of Na_V localization at peripheral end organs compared to central circuits. Only one of the monosynaptic reflex parameters changed across postnatal development in $Na_V1.6^{fl/fl}$ mice, response latency, which was faster at P14 to P18 compared to that at P6 to P11 (table S1). We predict that this is a result of activity dependent changes in primary afferent myelination (*57*), which is likely impaired in $Na_V1.6^{het}$ and $Na_V1.6^{cKO}$ mice.

We find that loss of $Na_V1.6$, but not $Na_V1.1$, resulted in disrupted muscle spindle development. This is in line with recent findings that show mechanosensory neuron end organ development is activity dependent (*21*). Previous work found deletion of Piezo2 in proprioceptors did not alter muscle spindle structure (*5*); however, these experiments were carried out in 4- to 5-week-old mice, whereas our analysis of muscle spindle structure was carried out in mice ages 8 to 12 weeks. This raises the possibility that electrical activity is required for the maintenance, but not development, of muscle spindle structure. We did note potentially reduced VGLUT1 immunolabeling in $Na_V1.6^{cKO}$ muscle spindle afferent endings (Fig. 6). Quantifying VGLUT1 expression in proprioceptor afferent endings is challenging, and analysis of protein expression via immunolabeling is not reliable or sufficiently quantitative. Reduced levels of VGLUT1 in muscle spindle afferents has been shown to decrease firing during static stretch (*58*). Whether this is contributing to loss of activity in $Na_V1.6^{cKO}$ mice is unclear. However, our analysis of muscle spindle structure is not compromised by changes in VGLUT1 expression as analysis using pan neuronal marker, βIII-tubulin, also found a significant decrease in WEI (fig. S6).

Unexpectedly, $Na_V1.6^{cKO}$ mice showed significantly reduced skeletal muscle fiber size, highlighting a potential non–cell-autonomous role for proprioceptive feedback in skeletal muscle development or maintenance (Figs. 7 and 10). This effect was not seen in $Na_V1.1^{cKO}$ mice but is consistent with a study that found deletion of Piezo2 in proprioceptors led to non–cell-autonomous deficits in spine alignment and hip joint formation (*59*). This marked reduction in myofiber area is impressive, as $Na_V1.6^{cKO}$ mice have severe motor impairments but are not immobile; our open-field data show that the amount of time $Na_V1.6^{cKO}$ mice spent moving was not statistically different from that of $Na_V1.6^{het}$ and $Na_V1.6^{fl/fl}$ mice. Moreover, prior work examining hindlimb unloading find a ~30 to 40% decrease in myofiber size over the course of 2 weeks of unloading (*60*), and unloading has a stronger effect on slow-twitch myofibers that are activated more regularly (*61*). We observe an even more pronounced effect on myofiber size in $Na_V1.6^{cKO}$ mice, and we also observe a clear reduction in the size of both slow- and fast-twitch myofiber fibers in $Na_V1.6^{cKO}$ mice. Thus, we propose that the lack of proprioceptive feedback in this model has non–cell-autonomous consequences on skeletal muscle that are independent of muscle unloading.

Despite the smaller size of $Na_V1.6^{cKO}$ skeletal muscle fibers, all $Na_V1.6^{cKO}$ intrinsic muscle properties were similar to $Na_V1.6^{het}$ and $Na_V1.6^{fl/fl}$ mice. Grip strength in $Na_V1.6^{cKO}$ mice, however, was significantly weaker compared to that in other genotypes. These findings suggest that reduced grip strength in $Na_V1.6^{cKO}$ mice is likely due to impaired motor neuron activation of skeletal muscle and not due to changes in intrinsic muscle function. The exact mechanism that leads to impaired motor neuron activation remains an open question. One possibility is that loss of proprioceptive feedback affects motor neuron excitability. Prior studies have identified dysfunction in proprioceptive spinal cord circuits in mouse models of spinal muscular atrophy and amyotrophic lateral sclerosis, neurodegenerative diseases in which motor neuron function is compromised (*19*, *62*–*64*). Moreover, restoration of survival motor neuron 1 gene in proprioceptors regulates the passive membrane properties of motor neurons in a mouse model of spinal muscular atrophy (*64*). An intriguing hypothesis is that loss of proprioceptive feedback onto motor neurons in $Na_V1.6^{cKO}$ mice (Fig. 4) results in pathophysiological phenotypes similar to those observed in neuromuscular or motor neuron disease.

Mutations in the genes that encode $Na_V1.1$ and $Na_V1.6$, *Scn1a* and *Scn8a*, respectively, are strongly associated with neurological diseases in which ataxia and motor developmental delays are prominent clinical manifestations (*12*, *26*, *50*). How proprioceptor dysfunction contributes to these disorders is unknown. Most patients with Dravet syndrome have complete LOF of one copy of *Scn1a*; conversely, patient reported mutational variants in *Scn8a* are predominately GOF. Our previous work found that proprioceptor afferents from $Na_V1.1^{het}$ mice also had impaired encoding static muscle stretch (*7*), suggesting that motor dysfunction in patients with Dravet syndrome missing one functional copy of *Scn1a* could be, in part, sensory in nature; however, it is unclear how *Scn8a* GOF mutations would affect proprioceptor function. Patients harboring either *Scn1a* LOF or *Scn8a* GOF mutations have similar motor deficits (*11*); thus, one possibility is that *Scn8a* GOF mutations lead to use-dependent block of action potential firing in proprioceptors, which could contribute to the similar motor phenotypes observed in these different patient populations (*11*). There are a few reported cases of LOF mutations in *Scn8a* that lead to general ataxia (*65*), and our data suggest that proprioceptor dysfunction could contribute to their motor deficits.

In addition to $Na_V1.1$ and $Na_V1.6$, proprioceptors also express $Na_V1.7$ (*7*). Mice and humans that lack $Na_V1.7$ are insensitive to pain but do not exhibit prominent deficits in motor function, which suggests a limited role of $Na_V1.7$ in mammalian proprioception (*9*, *10*). Alternatively, $Na_V1.1$ and $Na_V1.6$ may compensate for the developmental loss of $Na_V1.7$, which occurs in constitutive genetic mouse models and human patients. It is possible that acute deletion of $Na_V1.7$ in proprioceptors could reveal a previously overlooked contribution of the channel to proprioceptor function. We found that $Na_V1.7$ channels contribute to roughly one third of the somal whole-cell sodium current in genetically identified proprioceptors (*7*). Thus, a role for $Na_V1.7$ in mammalian proprioception remains enigmatic.

A current limitation of the present study is the use of a sensory-neuron wide genetic targeting strategy, which makes interpretation of motor behavior and skeletal muscle impairments confounded by the loss of $Na_V1.1$ or $Na_V1.6$ in other sensory neuron populations, namely, touch receptors. As mentioned above, deletion of $Na_V1.1$ or $Na_V1.6$ selectively in proprioceptors is not possible with now available genetic tools, as the access point for Cre-driven deletion, parvalbumin, is also expressed in neurons of brain and spinal cord that are important for motor function. Despite this limitation, the direct role of $Na_V1.1$ and $Na_V1.6$ in proprioceptors was examined at the functional level in ex vivo muscle nerve recordings and spinal cord electrophysiology experiments, as well as in the structural analysis of VGLUT1-identified muscle spindles. To investigate the role of Na_V channels with spatial precision, future experiments will require intersectional strategies for selective gene manipulations in proprioceptors.

Genetic and pharmacological studies have revealed how different Na_V channel subtypes encode distinct somatosensory modalities. For example, deletion of $Na_V1.7$ and $Na_V1.8$ eliminates noxious mechanical pain (*66*–*68*), and pharmacological activation of $Na_V1.1$ was shown promote mechanical pain but not pain induced by noxious heat (*69*). Furthermore, pharmacological inhibition of $Na_V1.6$ with μ-conotoxin GIIIA decreases oxaliplatin-induced cold allodynia, suggesting a role for $Na_V1.6$ in cold pain (*70*). While studies like these demonstrate the contributions of different Na_V subtypes across distinct somatosensory modalities, how the ensemble of Na_Vs expressed within a specific sensory neuron population shape electrical signaling and thus behavior has not been shown. Our data demonstrate that $Na_V1.1$ and $Na_V1.6$ play distinct and nonredundant roles in mammalian proprioceptors. This work defines how Na_Vs uniquely shape signaling within a discrete somatosensory modality and also shows that Na_Vs occupy distinct cellular compartments in sensory neuron end organs. We predict that our results are broadly applicable to other sensory neuron populations, namely, mechanoreceptors, which also co-express $Na_V1.1$ and $Na_V1.6$ (*39*). Furthermore, these data have important translational implications for understanding the motor deficits associated with $Na_V1.1$ and $Na_V1.6$ channelopathies.

MATERIALS AND METHODS

Experimental design

Animals

$Pirt^{cre}$ and $Scn8a^{fl/fl}$ mice were a gift from X. Dong [Johns Hopkins University; (*71*)] and M. Meisler [University of Michigan; (*72*)], respectively. $Scn1a^{fl/fl}$ mice (stock no. 041829-UCD) were purchased from the University of California, Davis (UC Davis) Mutant Mouse Resource and Research Center. All mice used are a C57BL/6J background (non-congenic). Genotyping was outsourced to Transnetyx. Animal use was conducted according to guidelines from the National Institutes of Health's *Guide for the Care and Use of Laboratory Animals* and was approved by the Institutional Animal Care and Use Committee of UC Davis (no. 23049) and San Jose State University (no. 990; ex vivo muscle recordings). $Na_V1.6^{cKO}$ mice were provided with wet food and hydrogels daily. Mice were maintained on a 12-hour light/dark cycle, and food and water were provided ad libitum.

Animal behavior

Motor function was tested using three assays: rotarod, open field, and grip strength. Behavioral assays were conducted from least to most invasive in the order of open field, grip strength, and rotarod. All behavioral assays were conducted between 8 and 10 weeks of age, and the experimenter was blind to genotype. For the open field, mice were acclimated to the behavior room for 1 hour prior testing. The open-field apparatus consisted of a white square box with dimensions of 15 inches (38.1 cm) by 15 inches (38.1 cm) by 20 inches

(50.8 cm). A camera suspended above the open field tracked animal movement for a single 10-min period using ANY-maze software. Following testing in the open field, mice were transported to a separate behavior room and allowed to acclimate for 1 hour before being assayed in the grip strength and rotarod tests. A grip strength apparatus (IITC Life Science, Woodland Hills, CA) with a metal grate was used. Mice held from the tail were placed on the metal grate and pulled horizontally away from apparatus once all four paws touched the grate. Mice were assayed across six trials with 5-min intervals between trials. A rotarod machine (IITC) that has an accelerating rotating cylinder was used. $Na_V1.6^{cKO}$ mice were excluded from rotarod testing because of severe motor coordination deficits that prevented them from maintaining balance on the cylinder even in the absence of cylinder rotation. The averages of three trials across three consecutive training days were recorded.

Ex vivo muscle nerve recordings

Detailed methods on ex vivo muscle nerve recordings can be found in (*16*). Briefly, extensor digitorum muscle and innervating peroneal branch of the sciatic nerve were dissected from adult mice and placed in a tissue bath of oxygenated synthetic interstitial fluid at 24°C. Tendons were tied to a fixed post and lever arm of a dual force and length controller and transducer (300C-LR, Aurora Scientific Inc.). The cut end of the nerve was suctioned into a bipolar glass electrode and connected to an extracellular amplifier with headstage (Model 1800, A-M Systems). Muscles were held at the length of maximal twitch contraction, Lo. For static stretch experiments, nine 4-s ramp-and-hold stretches were given at 2.5, 5, and 7.5% of Lo (ramp speed was 40% of Lo/s). Stretch lengths were repeated three times. For sinusoidal stimuli, 16 9-s sinusoidal vibrations were given at 5-, 25-, 50-, and 100-μm amplitudes at varying frequencies (10, 25, 50, and 100 Hz). A rest period of 1 min was given between each length change. Resting discharge was quantified as the firing rate 10 s before stretch. Firing rate during the static phase of stretch was calculated 3.25 to 3.75 s into the hold phase of stretch (LabChart software, ADInstruments). The consistency of firing during static muscle stretch was found by calculating the interspike interval coefficient of variation during the plateau phase of stretch (CV = SD/mean of ISI 1.5 to 3.5 s after ramp up). For dynamic responses, the average firing rates during the 9-s vibration were determined. Entrainment was defined as whether a unit could entrain in a 1:1 fashion to vibration stimulus. In most afferents, we confirmed that they were group Ia or II afferents by looking for a pause in firing during the shortening phase of contraction [a train of 60 stimulations of 0.5-ms pulse width was given at 1-Hz frequency from a 701C stimulator (Aurora Scientific)].

Spinal cord electrophysiology

Spinal cords were harvested from postnatal mice spanning the age groups P6 to P11 and P14 to P18. The mice were deeply anesthetized with isoflurane, decapitated, and eviscerated. We followed the protocol that has been used to record motor activity from mice of weight-bearing age using ex vivo spinal cord preparations (*73*, *74*). In brief, after evisceration, the preparation was pinned to a dissecting chamber and continuously perfused with ice-cold solution, comprising: 188 mM sucrose, 25 mM NaCl, 1.9 mM KCl, 10 mM $MgSO_4$, 0.5 mM NaH_2PO_4, 26 mM $NaHCO_3$, 1.2 mM NaH_2PO_4, 25 mM glucose, bubbled with 95% O_2/5% CO_2. The spinal cord was exposed following a ventral laminectomy and transected at the thoracic levels (T5-T8). The dorsal and ventral roots were isolated over the sixth lumbar segment, bilaterally, just proximal to the DRG. All other dorsal and ventral roots were trimmed, and the entire cord was removed from the vertebral column together with the attached roots and transferred to the recording chamber and continuously superfused with artificial cerebrospinal fluid (aCSF): 128 mM NaCl, 4 mM KCl, 1.5 mM $CaCl_2$, 1 mM $MgSO_4$, 0.5 mM NaH_2PO_4, 21 mM $NaHCO_3$, 30 mM D-glucose, bubbled with 95% O_2/5% CO_2. A midsagittal hemisection was performed, and the spinal hemicords were allowed to equilibrate in aCSF maintained at ambient temperature. After spinal cord isolation, dorsal and ventral roots at the sixth lumbar segment (L6) were placed into suction electrodes. The dorsal root was stimulated with single-pulse stimulus, delivered every 30 s, over 10 trials. The stimulus was delivered using a stimulus isolator unit (A365, World Precision Instruments) with current pulse amplitudes set at twice the threshold intensity of stimulation (2 T, 0.1-ms pulse width). Extracellular recordings were made at the ventral roots, and the signal was filtered between 0.1 and 5000 Hz, amplified 1000 times (Model 1700, A-M Systems), digitized at 10 kHz using Digidata 1440A, acquired using Clampex software (v11.2, Molecular Devices), and saved on a computer for offline analysis. Stretch reflex parameters were extracted from the signals for each experiment, after averaging over the 10 trials, using Clampfit (v11.2, Molecular Devices).

Muscle mechanics

Soleus muscles were prepared for ex vivo passive mechanical testing as previously described (*75*). Briefly, 7-0 sutures were cinched at the muscle-tendon of the soleus and EDL muscles. Suture loops were placed on hooks connected to the 300C-LR-Dual-Mode motor arm and force transducer (Aurora Scientific) such that the muscle remained within 28°C oxygenated Ringer's solution. Twitches were induced using a 701C stimulator (Aurora Scientific) across a range of muscle lengths to determine the optimal length for isometric force generation (Lo). The Lo length corresponded to the length between the sutures on either muscle-tendon junction, as measured by calipers. Physiological cross-sectional area (PCSA) was calculated using the muscle length (Lm), mass (m), ratio of fiber length to Lo (Lf/Lo), and standard density of muscle ($\rho = 1.06$ g/cm^3; PCSA = m/Lo*(Lf/Lo)*ρ (*76*).

Soleus muscles were subjected to active mechanical testing, which consisted of a series of 24 maximum isometric tetani (300 mA, 0.3-ms pulse width, 80-Hz pulse frequency, 800-ms pulse train) with 6 s of recovery in between each tetanus. Muscles were then given 300 s to recover before a final tetanus with the same parameters. Maximum isometric force was measured during the first, penultimate, and final tetanus protocol. Maximum forces were normalized to PCSA to give isometric specific tension. The highest isometric specific tension measured during each active protocol was reported as the isometric specific tension for each muscle. The percent of force maintained at the penultimate tetanus compared to the initial tetanus was recorded as the percent force after fatigue. The percent of force maintained at the final tetanus compared to the initial tetanus was recorded as the percent force after recovery. After active mechanical testing was completed, muscles were removed from the mechanical testing equipment, embedded in optimal cutting temperature (OCT) compound, and flash frozen in liquid nitrogen cooled isopentane. Muscles were stored at −70°C until cryosectioning.

Tissue processing

For muscle spindle immunolabeling experiments, mice were anesthetized using a ketamine/xylazine cocktail and transcardially perfused with phosphate-buffered saline (PBS) followed by 1%

paraformaldehyde (PFA). EDL muscle was then dissected in PBS, post-fixed for 30 min, and then washed in PBS before incubation in 30% sucrose solution overnight at 4°C. Following cryoprotection, muscles were embedded in optimal cutting temperature (Thermo Fisher Scientific, no. 4585) and stored in −80°C until sectioning.

Immunohistochemistry

For immunolabeling experiments in muscle spindles, EDL muscles were sectioned (30 μm) along the longitudinal axis. Tissue was incubated in blocking solution (0.1% PBS-Triton-X/5% normal goat serum in PBS), and the following primary antibodies were used: guinea pig anti-VGLUT1 (1:8000; Zuckerman Institute, 1705) and rabbit anti-βIII tubulin (1:3000; Abcam, no. ab18207). Secondary antibodies are as follows: anti–guinea pig 488 (1:1000; Thermo Fisher Scientific, A11073) and anti-rabbit 647 (1:1000, A32733). For muscle fiber typing experiments, soleus cross sections (20 μm) were blocked in a solution containing 5% bovine serum albumin (BSA) in PBS. The following primary antibodies were diluted and incubated on muscle sections overnight: mouse immunoglobulin G2b (IgG2b) anti-myosin heavy-chain type I [1:250; Developmental Studies Hybridoma Bank (DSHB), BA-F8] and mouse IgG1 anti-myosin heavy-chain type IIa (1:250; DSHB, SC-71). Slides were washed in PBS, and the following secondary antibodies were diluted in 2% BSA and incubated for 60 min: goat anti-mouse IgG2b 488 (1:500, A21141) goat anti-mouse IgG1 555 (1:500, A21127). After secondary antibody incubation, slides were washed in PBS and mounted with FluoromountG with DAPI (SouthernBiotech, 0100-20). For immunolabeling of Na_Vs, the following primary antibodies were used: guinea pig anti-VGLUT1 (1:8000; Zuckerman Institute, 1705), rabbit anti-$Na_V1.1$ (2 μg/ml; Neuromab, A11954), mouse IgG1 anti-$Na_V1.6$ (6 μg/ml, Neuromab K87A/10.2), rabbit anti-$Na_V1.6$ (1:750; Alomone, ASC009), IgG2a anti-AnkG (6 μg/ml, N106/36.1), and chicken anti-neurofilament heavy (1:3000; Abcam, ab4680). Secondary antibodies used were as follows: anti–guinea pig 488 (1:1000; Thermo Fisher Scientific, A11073), mouse anti-IgG1 555 (1:1000, A21137), mouse anti-IgG2a 647 (1:1000, A21240), and anti-chicken 594 (1:1000, WA316328). All specimens were imaged in three dimensions on either a Zeiss LSM 880 Airyscan [63× oil objective, 1.4 numerical aperture (NA)] or Olympus LV3000 (60× oil objective, 1.4 NA) confocal microscope. Images were analyzed using ImageJ software.

Analysis of muscle spindle structure

Disruptions in muscle spindle sensory endings were quantified by colocalizing VGLUT1 immunoreactivity with DAPI to calculate a WEI. Intrafusal muscle fibers are identifiable in skeletal muscle based on mono- and bi-nucleation via $DAPI^+$ staining. To analyze muscle spindle sensory wrappings without bias, we only analyzed sensory wrappings VGLUT1 sensory wrappings that overlapped with DAPI labeling. For example, in ImageJ, regions of interest (ROIs) were drawn around each sensory wrapping. If the ROI did not overlap with DAPI, then it was not counted as a sensory wrapping and was excluded from the analysis. The total number of sensory wrappings (n) was counted and normalized to muscle spindle length (l). The following equation was used to calculate the WEI

$$\mathrm{WEI} = n/\mathrm{l}$$

Experimental design and statistical analysis

Summary data are presented as means ± SD, from n cells, afferents, sections, or N animals. All analysis of immunofluorescent images contained at least three biological replicates per condition. Investigator was blinded to genotypes during analysis. For all behavioral, electrophysiological, and mechanics experiments, the investigator was blind to genotype. To determine differences in entrainment properties between $Na_V1.6^{fl/fl}$, $Na_V1.6^{het}$, and $Na_V1.6^{cKO}$, we used a logistic regression analysis (SPSS), which is a statistical model that calculates the log-odds of an event (i.e., entrainment or non-entrainment) as a linear combination of one or more independent variables (vibration frequency, vibration amplitude, and genotype). All other statistical testing was carried out using Prism 10.1 (GraphPad software). Statistical differences were determined using parametric tests for normally distributed data and nonparametric tests for data that did not conform to Gaussian distributions or had different variances. Statistical significance in each case is denoted as follows: $*P < 0.05$, $**P < 0.01$, $***P < 0.001$, and $****P < 0.0001$. Source files for each figure can be found on Mendeley.

Supplementary Materials

The PDF file includes:

Supplementary Methods
Figs. S1 to S10
Table S1
Legends for movies S1 and S2

Other Supplementary Material for this manuscript includes the following:

Movies S1 and S2

REFERENCES AND NOTES

1. U. Proske, S. C. Gandevia, The proprioceptive senses: Their roles in signaling body shape, body position and movement, and muscle force. *Physiol. Rev.* **92**, 1651–1697 (2012).
2. J. C. Tuthill, E. Azim, Proprioception. *Curr. Biol.* **28**, R194–R203 (2018).
3. K. A. Wilkinson, Molecular determinants of mechanosensation in the muscle spindle. *Curr. Opin. Neurobiol.* **74**, 102542 (2022).
4. D. Florez-Paz, K. K. Bali, R. Kuner, A. Gomis, A critical role for Piezo2 channels in the mechanotransduction of mouse proprioceptive neurons. *Sci. Rep.* **6**, 25923 (2016).
5. S.-H. Woo, V. Lukacs, J. C. de Nooij, D. Zaytseva, C. R. Criddle, A. Francisco, T. M. Jessell, K. A. Wilkinson, A. Patapoutian, Piezo2 is the principal mechanotransduction channel for proprioception. *Nat. Neurosci.* **18**, 1756–1762 (2015).
6. A. T. Chesler, M. Szczot, D. Bharucha-Goebel, M. Čeko, S. Donkervoort, C. Laubacher, L. H. Hayes, K. Alter, C. Zampieri, C. Stanley, A. M. Innes, J. K. Mah, C. M. Grosmann, N. Bradley, D. Nguyen, A. R. Foley, C. E. Le Pichon, C. G. Bönnemann, The Role of PIEZO2 in Human Mechanosensation. *N. Engl. J. Med.* **375**, 1355–1364 (2016).
7. C. M. Espino, C. M. Lewis, S. Ortiz, M. S. Dalal, S. Garlapalli, K. M. Wells, D. A. O'Neil, K. A. Wilkinson, T. N. Griffith, $Na_V1.1$ is essential for proprioceptive signaling and motor behaviors. *eLife* **11**, e79917 (2022).
8. S. D. Dib-Hajj, A. M. Rush, T. R. Cummins, F. M. Hisama, S. Novella, L. Tyrrell, L. Marshall, S. G. Waxman, Gain-of-function mutation in $Na_v1.7$ in familial erythromelalgia induces bursting of sensory neurons. *Brain* **128**, 1847–1854 (2005).
9. J. J. Cox, F. Reimann, A. K. Nicholas, G. Thornton, E. Roberts, K. Springell, G. Karbani, H. Jafri, J. Mannan, Y. Raashid, L. Al-Gazali, H. Hamamy, E. M. Valente, S. Gorman, R. Williams, D. P. McHale, J. N. Wood, F. M. Gribble, C. G. Woods, An *SCN9A* channelopathy causes congenital inability to experience pain. *Nature* **444**, 894–898 (2006).
10. J. Gingras, S. Smith, D. J. Matson, D. Johnson, K. Nye, L. Couture, E. Feric, R. Yin, B. D. Moyer, M. L. Peterson, J. B. Rottman, R. J. Beiler, A. B. Malmberg, S. I. McDonough, Global Nav1.7 knockout mice recapitulate the phenotype of human congenital indifference to pain. *PLOS ONE* **9**, e105895 (2014).
11. M. H. Meisler, S. F. Hill, W. Yu, Sodium channelopathies in neurodevelopmental disorders. *Nat. Rev. Neurosci.* **22**, 152–166 (2021).
12. M. H. Meisler, J. Kearney, A. Escayg, B. T. MacDonald, L. K. Sprunger, Sodium channels and neurological disease: Insights from Scn8a mutations in the mouse. *Neuroscientist* **7**, 136–145 (2001).
13. S. I. Levin, Z. M. Khaliq, T. K. Aman, T. M. Grieco, J. A. Kearney, I. M. Raman, M. H. Meisler, Impaired motor function in mice with cell-specific knockout of sodium channel *Scn8a* ($Na_V1.6$) in cerebellar purkinje neurons and granule cells. *J. Neurophysiol.* **96**, 785–793 (2006).
14. I. Ogiwara, H. Miyamoto, N. Morita, N. Atapour, E. Mazaki, I. Inoue, T. Takeuchi, S. Itohara, Y. Yanagawa, K. Obata, T. Furuichi, T. K. Hensch, K. Yamakawa, $Na_v1.1$ localizes to axons of

parvalbumin-positive inhibitory interneurons: A circuit basis for epileptic seizures in mice carrying an *Scn1a* gene mutation. *J. Neurosci.* **27**, 5903–5914 (2007).
15. B. Ferguson, C. Glick, J. R. Huguenard, Prefrontal PV interneurons facilitate attention and are linked to attentional dysfunction in a mouse model of absence epilepsy. *eLife* **12**, e78349 (2023).
16. K. A. Wilkinson, H. E. Kloefkorn, S. Hochman, Characterization of muscle spindle afferents in the adult mouse using an in vitro muscle-nerve preparation. *PLOS ONE* **7**, e39140 (2012).
17. J. C. Eccles, R. M. Eccles, A. Lundberg, The convergence of monosynaptic excitatory afferents on to many different species of alpha motoneurones. *J. Physiol.* **137**, 22–50 (1957).
18. S. C. Mears, E. Frank, Formation of specific monosynaptic connections between muscle spindle afferents and motoneurons in the mouse. *J. Neurosci.* **17**, 3128–3135 (1997).
19. G. Z. Mentis, D. Blivis, W. Liu, E. Drobac, M. E. Crowder, L. Kong, F. J. Alvarez, C. J. Sumner, M. J. O'Donovan, Early functional impairment of sensory-motor connectivity in a mouse model of spinal muscular atrophy. *Neuron* **69**, 453–467 (2011).
20. K. M. Oliver, D. M. Florez-Paz, T. C. Badea, G. Z. Mentis, V. Menon, J. C. de Nooij, Molecular correlates of muscle spindle and Golgi tendon organ afferents. *Nat. Commun.* **12**, 1451 (2021).
21. C. Santiago, N. Sharma, N. Africawala, J. Siegrist, A. Handler, A. Tasnim, R. Anjum, J. Turecek, B. P. Lehnert, S. Renauld, M. Nolan-Tamariz, M. Iskols, A. R. Magee, S. Paradis, D. D. Ginty, Activity-dependent development of the body's touch receptors. bioRxiv 559109 [Preprint] (2023). https://doi.org/10.1101/2023.09.23.559109.
22. L. W. Duchen, E. Stefani, Electrophysiological studies of neuromuscular transmission in hereditary "motor end-plate disease" of the mouse. *J. Physiol.* **212**, 535–548 (1971).
23. L. R. Smith, E. R. Barton, SMASH - semi-automatic muscle analysis using segmentation of histology: A MATLAB application. *Skelet. Muscle* **4**, 21 (2014).
24. I. Kwon, K. S. Kim, Y. Lee, Relationships between endurance exercise training-induced muscle fiber-type shifting and autophagy in slow- and fast-twitch skeletal muscles of mice. *Phys. Act. Nutr.* **28**, 23–34 (2024).
25. N. Haida, W. M. Fowler Jr., R. T. Abresch, D. B. Larson, R. B. Sharman, R. G. Taylor, R. K. Entrikin, Effect of hind-limb suspension on young and adult skeletal muscle. I. Normal mice. *Exp. Neurol.* **103**, 68–76 (1989).
26. F. Kalume, F. H. Yu, R. E. Westenbroek, T. Scheuer, W. A. Catterall, Reduced sodium current in Purkinje neurons from $Na_v1.1$ mutant mice: Implications for ataxia in severe myoclonic epilepsy in infancy. *J. Neurosci.* **27**, 11065–11074 (2007).
27. R. R. Patel, C. Barbosa, Y. Xiao, T. R. Cummins, Human Nav1.6 channels generate larger resurgent currents than human Nav1.1 channels, but the Navβ4 peptide does not protect either isoform from use-dependent reduction. *PLOS ONE* **10**, e0133485 (2015).
28. Z. M. Khaliq, N. W. Gouwens, I. M. Raman, The contribution of resurgent sodium current to high-frequency firing in Purkinje neurons: An experimental and modeling study. *J. Neurosci.* **23**, 4899–4912 (2003).
29. W. Hu, C. Tian, T. Li, M. Yang, H. Hou, Y. Shu, Distinct contributions of Na(v)1.6 and Na(v)1.2 in action potential initiation and backpropagation. *Nat. Neurosci.* **12**, 996–1002 (2009).
30. A. Duflocq, B. Le Bras, E. Bullier, F. Couraud, M. Davenne, Nav1.1 is predominantly expressed in nodes of Ranvier and axon initial segments. *Mol. Cell. Neurosci.* **39**, 180–192 (2008).
31. J. H. Caldwell, K. L. Schaller, R. S. Lasher, E. Peles, S. R. Levinson, Sodium channel Na(v)1.6 is localized at nodes of Ranvier, dendrites, and synapses. *Proc. Natl. Acad. Sci. U.S.A.* **97**, 5616–5620 (2000).
32. E. J. Akin, L. Solé, S. D. Dib-Hajj, S. G. Waxman, M. M. Tamkun, Preferential targeting of $Na_v1.6$ voltage-gated Na^+ channels to the axon initial segment during development. *PLOS ONE* **10**, e0124397 (2015).
33. A. N. King, C. F. Manning, J. S. Trimmer, A unique ion channel clustering domain on the axon initial segment of mammalian neurons. *J. Comp. Neurol.* **522**, 2594–2608 (2014).
34. G. S. Bewick, R. W. Banks, Mechanotransduction in the muscle spindle. *Pflugers Arch.* **467**, 175–190 (2015).
35. B. Bornstein, B. Watkins, F. S. Passini, R. Blecher, E. Assaraf, X. M. Sui, V. Brumfeld, M. Tsoory, S. Kröger, E. Zelzer, The mechanosensitive ion channel ASIC2 mediates both proprioceptive sensing and spinal alignment. *Exp. Physiol.* **109**, 135–147 (2024).
36. S.-H. Lin, Y.-R. Cheng, R. W. Banks, M.-Y. Min, G. S. Bewick, C.-C. Chen, Evidence for the involvement of ASIC3 in sensory mechanotransduction in proprioceptors. *Nat. Commun.* **7**, 11460 (2016).
37. J. F. Madden, O. C. Davis, K. A. Boyle, J. A. Iredale, T. J. Browne, R. J. Callister, D. W. Smith, P. Jobling, D. I. Hughes, B. A. Graham, Functional and molecular analysis of proprioceptive sensory neuron excitability in mice. *Front. Mol. Neurosci.* **13**, 36 (2020).
38. W. P. Mayer, A. J. Murray, S. Brenner-Morton, T. M. Jessell, W. G. Tourtellotte, T. Akay, Role of muscle spindle feedback in regulating muscle activity strength during walking at different speed in mice. *J. Neurophysiol.* **120**, 2484–2497 (2018).
39. Y. Zheng, P. Liu, L. Bai, J. S. Trimmer, B. P. Bean, D. D. Ginty, Deep sequencing of somatosensory neurons reveals molecular determinants of intrinsic physiological properties. *Neuron* **103**, 598–616.e7 (2019).
40. S. C. Koch, M. G. Del Barrio, A. Dalet, G. Gatto, T. Günther, J. Zhang, B. Seidler, D. Saur, R. Schüle, M. Goulding, RORβ spinal interneurons gate sensory transmission during locomotion to secure a fluid walking gait. *Neuron* **96**, 1419–1431.e5 (2017).
41. M. A. Gradwell, N. Ozeri-Engelhard, J. T. Eisdorfer, O. D. Laflamme, M. Gonzalez, A. Upadhyay, L. Medlock, T. Shrier, K. R. Patel, A. Aoki, M. Gandhi, G. Abbas-Zadeh, O. Oputa, J. K. Thackray, M. Ricci, A. George, N. Yusuf, J. Keating, Z. Imtiaz, S. A. Alomary, M. Bohic, M. Haas, Y. Hernandez, S. A. Prescott, T. Akay, V. E. Abraira, Multimodal sensory control of motor performance by glycinergic interneurons of the mouse spinal cord deep dorsal horn. *Neuron* **112**, 1302–1327.e13 (2024).
42. S. Kröger, B. Watkins, Muscle spindle function in healthy and diseased muscle. *Skelet. Muscle* **11**, 3 (2021).
43. J. Desaki, N. Nishida, A further observation of muscle spindles in the extensor digitorum longus muscle of the aged rat. *J. Electron Microsc. (Tokyo)* **59**, 79–86 (2010).
44. L. Gerwin, S. Rossmanith, C. Haupt, J. Schultheiß, H. Brinkmeier, R. E. Bittner, S. Kröger, Impaired muscle spindle function in murine models of muscular dystrophy. *J. Physiol.* **598**, 1591–1609 (2020).
45. T. N. Griffith, T. A. Docter, E. A. Lumpkin, Tetrodotoxin-sensitive sodium channels mediate action potential firing and excitability in menthol-sensitive Vglut3-lineage sensory neurons. *J. Neurosci.* **39**, 7086–7101 (2019).
46. B. Drouillas, C. Brocard, S. Zanella, R. Bos, F. Brocard, Persistent Nav1.1 and Nav1.6 currents drive spinal locomotor functions through nonlinear dynamics. *Cell Rep.* **42**, 113085 (2023).
47. J. E. O'Brien, M. H. Meisler, Sodium channel SCN8A (Nav1.6): Properties and de novo mutations in epileptic encephalopathy and intellectual disability. *Front. Genet.* **4**, 213 (2013).
48. T. Boiko, A. Van Wart, J. H. Caldwell, S. R. Levinson, J. S. Trimmer, G. Matthews, Functional specialization of the axon initial segment by isoform-specific sodium channel targeting. *J. Neurosci.* **23**, 2306–2313 (2003).
49. D. P. Schafer, A. W. Custer, P. Shrager, M. N. Rasband, Early events in node of Ranvier formation during myelination and remyelination in the PNS. *Neuron Glia Biol.* **2**, 69–79 (2006).
50. F. H. Yu, M. Mantegazza, R. E. Westenbroek, C. A. Robbins, F. Kalume, K. A. Burton, W. J. Spain, G. S. McKnight, T. Scheuer, W. A. Catterall, Reduced sodium current in GABAergic interneurons in a mouse model of severe myoclonic epilepsy in infancy. *Nat. Neurosci.* **9**, 1142–1149 (2006).
51. S. R. Stevens, M. N. Rasband, Ankyrins and neurological disease. *Curr. Opin. Neurobiol.* **69**, 51–57 (2021).
52. C. Zhang, A. Joshi, Y. Liu, O. Sert, S. G. Haddix, L. H. Teliska, A. Rasband, G. G. Rodney, M. N. Rasband, Ankyrin-dependent Na^+ channel clustering prevents neuromuscular synapse fatigue. *Curr. Biol.* **31**, 3810–3819.e4 (2021).
53. A. Van Wart, T. Boiko, J. S. Trimmer, G. Matthews, Novel clustering of sodium channel Na(v)1.1 with ankyrin-G and neurofascin at discrete sites in the inner plexiform layer of the retina. *Mol. Cell. Neurosci.* **28**, 661–673 (2005).
54. F. Laezza, B. R. Gerber, J.-Y. Lou, M. A. Kozel, H. Hartman, A. M. Craig, D. M. Ornitz, J. M. Nerbonne, The $FGF14^{F145S}$ mutation disrupts the interaction of FGF14 with voltage-gated Na^+ channels and impairs neuronal excitability. *J. Neurosci.* **27**, 12033–12044 (2007).
55. L. L. Isom, Sodium channel beta subunits: Anything but auxiliary. *Neuroscientist* **7**, 42–54 (2001).
56. S. Luo, M. Jaegle, R. Li, G. R. Ehring, D. Meijer, S. R. Levinson, The sodium channel isoform transition at developing nodes of Ranvier in the peripheral nervous system: Dependence on a Genetic program and myelination-induced cluster formation. *J. Comp. Neurol.* **522**, 4057–4073 (2014).
57. D. Kato, H. Wake, Activity-dependent myelination. *Adv. Exp. Med. Biol.* **1190**, 43–51 (2019).
58. K. Than, E. Kim, C. Navarro, S. Chu, N. Klier, A. Occiano, S. Ortiz, A. Salazar, S. R. Valdespino, N. K. Villegas, K. A. Wilkinson, Vesicle-released glutamate is necessary to maintain muscle spindle afferent excitability but not dynamic sensitivity in adult mice. *J. Physiol.* **599**, 2953–2967 (2021).
59. E. Assaraf, R. Blecher, L. Heinemann-Yerushalmi, S. Krief, R. Carmel Vinestock, I. E. Biton, V. Brumfeld, R. Rotkopf, E. Avisar, G. Agar, E. Zelzer, Piezo2 expressed in proprioceptive neurons is essential for skeletal integrity. *Nat. Commun.* **11**, 3168 (2020).
60. F. Wang, P. Zhang, H. Liu, M. Fan, X. Chen, Proteomic analysis of mouse soleus muscles affected by hindlimb unloading and reloading. *Muscle Nerve* **52**, 803–811 (2015).
61. Y. Gao, Y. Arfat, H. Wang, N. Goswami, Muscle atrophy induced by mechanical unloading: Mechanisms and potential countermeasures. *Front. Physiol.* **9**, 235 (2018).
62. M. A. Rubio, M. Herrando-Grabulosa, X. Navarro, Sensory involvement in amyotrophic lateral sclerosis. *Int. J. Mol. Sci.* **23**, 15521 (2022).
63. R. Aishwarya, C. S. Abdullah, N. S. Remex, S. Nitu, B. Hartman, J. King, M. A. N. Bhuiyan, O. Rom, S. Miriyala, M. Panchatcharam, A. W. Orr, C. G. Kevil, M. S. Bhuiyan, Pathological sequelae associated with skeletal muscle atrophy and histopathology in G93A*SOD1 mice. *Muscles* **2**, 51–74 (2023).
64. E. V. Fletcher, C. M. Simon, J. G. Pagiazitis, J. I. Chalif, A. Vukojicic, E. Drobac, X. Wang, G. Z. Mentis, Reduced sensory synaptic excitation impairs motor neuron function via Kv2.1 in spinal muscular atrophy. *Nat. Neurosci.* **20**, 905–916 (2017).
65. J. L. Wagnon, N. E. Mencacci, B. S. Barker, E. R. Wengert, K. P. Bhatia, B. Balint, M. Carecchio, N. W. Wood, M. K. Patel, M. H. Meisler, Partial loss-of-function of sodium channel *SCN8A* in familial isolated myoclonus. *Hum. Mutat.* **39**, 965–969 (2018).

66. M. A. Nassar, L. C. Stirling, G. Forlani, M. D. Baker, E. A. Matthews, A. H. Dickenson, J. N. Wood, Nociceptor-specific gene deletion reveals a major role for Nav1.7 (PN1) in acute and inflammatory pain. *Proc. Natl. Acad. Sci. U.S.A.* **101**, 12706–12711 (2004).
67. M. A. Nassar, A. Levato, L. C. Stirling, J. N. Wood, Neuropathic pain develops normally in mice lacking both Na(v)1.7 and Na(v)1.8. *Mol. Pain* **1**, 24 (2005).
68. A. N. Akopian, V. Souslova, S. England, K. Okuse, N. Ogata, J. Ure, A. Smith, B. J. Kerr, S. B. McMahon, S. Boyce, R. Hill, L. C. Stanfa, A. H. Dickenson, J. N. Wood, The tetrodotoxin-resistant sodium channel SNS has a specialized function in pain pathways. *Nat. Neurosci.* **2**, 541–548 (1999).
69. J. D. Osteen, V. Herzig, J. Gilchrist, J. J. Emrick, C. Zhang, X. Wang, J. Castro, S. Garcia-Caraballo, L. Grundy, G. Y. Rychkov, A. D. Weyer, Z. Dekan, E. A. B. Undheim, P. Alewood, C. L. Stucky, S. M. Brierley, A. I. Basbaum, F. Bosmans, G. F. King, D. Julius, Selective spider toxins reveal a role for the Nav1.1 channel in mechanical pain. *Nature* **534**, 494–499 (2016).
70. J. R. Deuis, K. Zimmermann, A. A. Romanovsky, L. D. Possani, P. J. Cabot, R. J. Lewis, I. Vetter, An animal model of oxaliplatin-induced cold allodynia reveals a crucial role for Nav1.6 in peripheral pain pathways. *Pain* **154**, 1749–1757 (2013).
71. A. Y. Kim, Z. Tang, Q. Liu, K. N. Patel, D. Maag, Y. Geng, X. Dong, Pirt, a phosphoinositide-binding protein, functions as a regulatory subunit of TRPV1. *Cell* **133**, 475–485 (2008).
72. S. I. Levin, M. H. Meisler, Floxed allele for conditional inactivation of the voltage-gated sodium channel Scn8a (NaV1.6). *Genesis* **39**, 234–239 (2004).
73. Z. Jiang, K. P. Carlin, R. M. Brownstone, An in vitro functionally mature mouse spinal cord preparation for the study of spinal motor networks. *Brain Res.* **816**, 493–499 (1999).
74. C. Nagaraja, Ventral root evoked entrainment of disinhibited bursts across early postnatal development in mice. *IBRO Rep.* **9**, 310–318 (2020).
75. R. P. Wohlgemuth, R. M. Feitzinger, K. E. Henricson, D. T. Dinh, S. E. Brashear, L. R. Smith, The extracellular matrix of dystrophic mouse diaphragm accounts for the majority of its passive stiffness and is resistant to collagenase digestion. *Matrix Biol Plus* **18**, 100131 (2023).
76. J. Mendez, A. Keys, Density and composition of mammalian muscle. *Metabolism* **9**, 184–188 (1960).

Acknowledgments: We would like to thank X. Dong and M. Meisler for sharing mouse lines and J. Trimmer for providing support and guidance on immunolabeling experiments. Last, thanks to Griffith and Contreras Lab members for helpful discussions. **Funding:** This study was supported by the National Institute General Medical Sciences (T32GM099608 and T32GM1144303, C.M.E.; R16GM153600, K.A.W.; and R25GM116690, E.L.M.), National Institute of Neurological Disease and Stroke (F31NS134241, C.M.E.; R25NS112130, Y.M.; R01NS135005, T.N.G.; and K01NS124828, T.N.G.), and the National Institute of Arthritis and Musculoskeletal and Skin Diseases (R01AR079545, L.R.S.; and F31AR082695, R.P.W.). Additional support was provided by The Doris Duke Charitable Foundation COVID-19 Fund to Retain Clinical Scientists awarded to UC Davis School of Medicine by the Burroughs Wellcome Fund (T.N.G.). Core facilities were supported by P30 EY12576. **Author contributions:** Conceptualization: C.M.E. and T.N.G. Methodology: C.M.E., C.N., J.R.D., L.R.S., K.A.W., and T.N.G. Validation: C.M.E., A.R.M., E.L.M., L.R.S., K.A.W., and T.N.G. Formal analysis: C.M.E., C.N., S.O., J.R.D., A.R.M., Y.M., E.L.M., S.G., R.P.W., S.E.B., L.R.S., K.A.W., and T.N.G. Investigation: C.M.E., C.N., S.O., J.R.D., A.R.M., Y.M., E.L.M., S.G., R.P.W., and S.E.B. Resources: L.R.S., K.A.W., and T.N.G. Data curation: C.M.E., L.R.S., K.A.W., and T.N.G. Writing—original draft: C.M.E. Writing—review and editing: C.M.E., C.N., S.O., J.R.D., A.R.M., Y.M., E.L.M., S.G., R.P.W., S.E.B., L.R.S., K.A.W., and T.N.G. Visualization: C.M.E. and T.N.G. Supervision: C.M.E., L.R.S., K.A.W., and T.N.G. Project administration: C.M.E., L.R.S., K.A.W., and T.N.G. Funding acquisition: C.M.E., R.P.W., L.R.S., K.A.W., and T.N.G. **Competing interests:** The authors declare that they have no competing interests. **Data and materials availability:** All data needed to evaluate the conclusions in the paper are present in the paper and/or the Supplementary Materials. Source data for each figure can be found on Mendeley (https://data.mendeley.com/preview/zw22vbkbp9?a=b943edc9-d5bc-4ba5-aed4-2f9892c19492).

Submitted 28 August 2024
Accepted 2 December 2024
Published 8 January 2025
10.1126/sciadv.ads6660